ARTICLES
https://doi.org/10.1038/s41588-020-00749-z

nature genetics

Genetic screening for single-cell variability modulators driving therapy resistance

Eduardo A. Torre[1], Eri Arai[2,10], Sareh Bayatpour[3,10], Connie L. Jiang[4,10], Lauren E. Beck[3], Benjamin L. Emert[5], Sydney M. Shaffer[3,6], Ian A. Mellis[5], Mitchell E. Fane[7], Gretchen M. Alicea[7], Krista A. Budinich[2], Ashani T. Weeraratna[7,8], Junwei Shi[2] ✉ and Arjun Raj[3,9] ✉

Cellular plasticity describes the ability of cells to transition from one set of phenotypes to another. In melanoma, transient fluctuations in the molecular state of tumor cells mark the formation of rare cells primed to survive BRAF inhibition and reprogram into a stably drug-resistant fate. However, the biological processes governing cellular priming remain unknown. We used CRISPR–Cas9 genetic screens to identify genes that affect cell fate decisions by altering cellular plasticity. We found that many factors can independently affect cellular priming and fate decisions. We discovered a new plasticity-based mode of increasing resistance to BRAF inhibition that pushes cells towards a more differentiated state. Manipulating cellular plasticity through inhibition of DOT1L before the addition of the BRAF inhibitor resulted in more therapy resistance than concurrent administration. Our results indicate that modulating cellular plasticity can alter cell fate decisions and may prove useful for treating drug resistance in other cancers.

Plasticity describes the ability of cells to transition from one phenotype to another, enabling cells to adapt and survive in the face of a variety of stimuli and challenges. Examples include regeneration, wound healing and the induction of pluripotency. Plasticity can be decomposed into stimulus-independent and subsequent stimulus-dependent phases. The first phase typically consists of (often rare) cells within the population being 'primed' for the cell fate transition. Then, upon the stimulus, these primed cells are selectively reprogrammed to adopt the new phenotype. A major question in single-cell biology has been determining the molecular differences specific to these primed cells and connecting those differences to their ultimate fate after the stimulus reprograms them. Recent studies have developed the link between cellular priming and cell fate that underlies plasticity in a number of contexts[1–8]. However, little is known about pathways that can manipulate the fluctuations that drive priming and whether those pathways can affect their subsequent fates, leaving potential therapeutic applications largely unrealized.

Therapy resistance in melanoma is an excellent example of cellular plasticity[9,10]. Therapies such as vemurafenib that inhibit particular oncogenic targets often kill most tumor cells, but a few remaining cells continue to proliferate, ultimately repopulating the tumor. While the mechanisms underlying this therapy resistance often emerge from a genetic mutation, many recent studies, both in melanoma and other cancers, suggest a role for nongenetic mechanisms driving cellular plasticity, in particular right after the application of therapy. Plasticity here refers to the rare cells that are transiently primed to survive drug treatment and are then reprogrammed into a more stably resistant state by the drug itself[8,11–21]. In melanoma, this primed cellular state, which we have also previously referred to as the pre-resistant cellular state, is often marked by transiently high expression of resistance marker genes such as *EGFR*, *NGFR* and *AXL* (Fig. 1a, top). Exposure to the drug reprograms these cells by converting the transiently primed phenotype into a stably drug-resistant phenotype characterized by massive changes in signaling and gene expression profiles (Note that if one removes drug from stably resistant cells for a period of 3 weeks, the cells are still completely resistant upon reexposure[14]). A notable difference between this paradigm of resistance and more conventional models of drug resistance caused by a mutation is that, while genetic mutations largely arise spontaneously, the nongenetic fluctuations driving primed states could result from the activity of specific biological pathways. Targeting these pathways could potentially enhance or inhibit the formation of primed cells in the primed state. We wanted to dissect the molecular regulators of priming and determine how they might affect the overall acquisition of resistance.

CRISPR–Cas9 technology enables genetic screens to identify regulators of such molecular processes. For most cell fate transitions, including therapy resistance, virtually all screens have been designed to detect changes to the ultimate fate only—that is, changes in the final number of resistant cells, typically measured as a proliferation phenotype[22–25]. However, such screens do not explicitly target priming, which may in principle have distinct regulatory mechanisms to those of the acquisition of resistance as a whole. These mechanisms may then also affect the overall degree of drug resistance, but potentially through new, previously undiscovered pathways that affect drug resistance in ways not revealed by classical resistance screens (Fig. 1a, bottom).

[1]Biochemistry and Molecular Biophysics Graduate Group, Perelman School of Medicine, University of Pennsylvania, Philadelphia, PA, USA. [2]Department of Cancer Biology, Perelman School of Medicine, University of Pennsylvania, Philadelphia, PA, USA. [3]Department of Bioengineering, School of Engineering and Applied Science, University of Pennsylvania, Philadelphia, PA, USA. [4]Genetics and Epigenetics, Cell and Molecular Biology Graduate Group, Perelman School of Medicine, University of Pennsylvania, Philadelphia, PA, USA. [5]Genomics and Computational Biology Graduate Group, Perelman School of Medicine, University of Pennsylvania, Philadelphia, PA, USA. [6]Department of Pathology and Laboratory Medicine, Perelman School of Medicine, University of Pennsylvania, Philadelphia, PA, USA. [7]Department of Biochemistry and Molecular Biology, Johns Hopkins School of Public Health, Baltimore, MD, USA. [8]Sidney Kimmel Cancer Center, Johns Hopkins School of Medicine, Baltimore, MD, USA. [9]Department of Genetics, Perelman School of Medicine, University of Pennsylvania, Philadelphia, PA, USA. [10]These authors contributed equally: Eri Arai, Sareh Bayatpour, Connie L. Jiang. ✉e-mail: jushi@upenn.edu; arjunraj@seas.upenn.edu

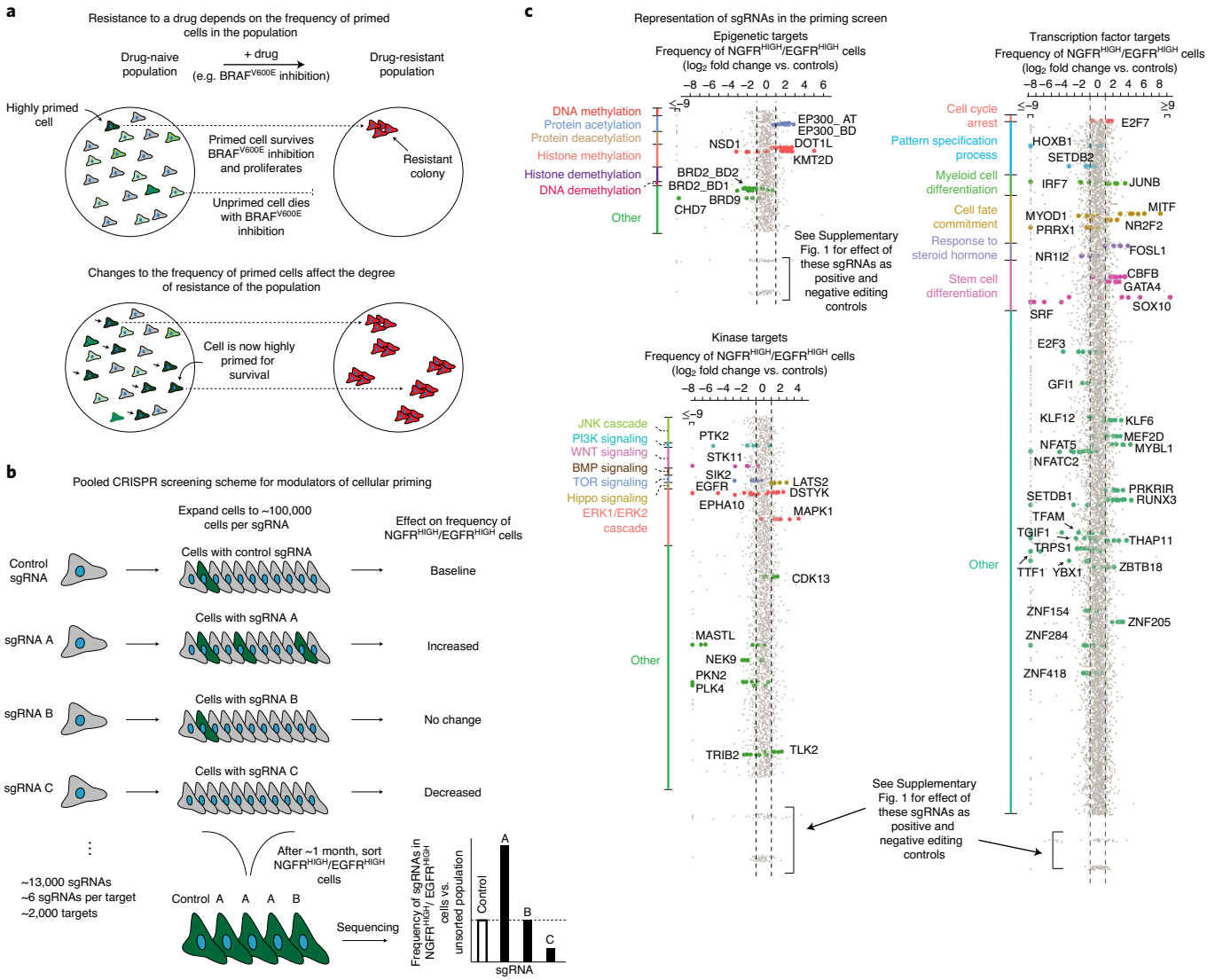

Fig. 1 | Pooled CRISPR screen design to identify modulators of cellular priming in the context of drug resistance to targeted therapies in melanoma. **a**, In melanoma, the initial molecular profile of a cell (primed (green) versus unprimed (gray)) within an otherwise homogeneous population dictates the ultimate fate of the cell (for example, proliferation versus death) when exposed to therapy (top). Changing the number of cells in a given state (bottom) can alter the number of resistant colonies that form upon addition of the $BRAF^{V600E}$ inhibitor vemurafenib. **b**, We designed a pooled CRISPR screen to detect modulators of the cellular priming that leads to drug resistance. After transducing a library of sgRNAs and expanding the population, we isolated cells with high expression of both NGFR and EGFR, then sequenced the sgRNAs to determine which gene knockouts altered the frequency of these cells. Changes in the frequency of a given sgRNA in this population (for example, targets A and C) indicate that these targets may affect the frequency of $NGFR^{HIGH}/EGFR^{HIGH}$ cells in the population, and thus may affect the frequency of cellular priming. **c**, After transducing a population of melanoma cells and isolating $NGFR^{HIGH}/EGFR^{HIGH}$ cells (see **b**), we quantified the frequency of each sgRNA in the resulting population. Our screening scheme used three separate pooled sgRNA libraries: one targeting epigenetic domains (top left), another targeting kinases (bottom left) and a final one targeting transcription factors (right). We organized the targets within each sgRNA library by biological process; while a given target could fall into several categories, each target was assigned to a single group and plotted only once. Each dot represents a sgRNA, grouped by gene target (5–6 sgRNAs per target), with the $\log_2$ fold change representing the number of times the sgRNA was detected in the sorted population versus an unsorted population of melanoma cells transduced with the same library. For display purposes, all sgRNAs with fold changes beyond the axis limits were placed at the edge of the axis as indicated. For targets considered 'hits' by our rubric (Methods), we labeled the sgRNA dot by the color assigned to that biological process. Dots at the bottom of each pane correspond to nontargeting controls (sgRNAs not targeting any loci in the genome) and cell viability controls (for example, proteins required for cell survival and proliferation, but not specifically associated with rare-cell behavior). Extended Data Fig. 2 provides details on the effect of these sgRNAs as positive and negative editing controls. BMP, bone morphogenetic protein; ERK, extracellular signal-regulated kinase; JNK, c-Jun N-terminal kinase; PI3K, phosphatidylinositol 3-kinase; TOR, target of rapamycin.

Here we performed pooled CRISPR–Cas9 genetic screens designed to capture modulators of priming for drug resistance in single melanoma cells. This screen identified several new factors that affect the frequency of primed cells in clonal melanoma populations and, consequently, resistance to targeted therapies. The transcriptome profiles induced by knocking out these factors revealed a new mechanism that can increase or reduce drug resistance by increasing or decreasing the activity of differentiation

pathways, respectively, as opposed to increasing drug resistance by decreasing differentiation. Drugs targeting these factors display a variety of synergistic effects when coupled with therapy, which can be dependent on the relative timing of drug application. Together, our results indicate that modulating cellular plasticity can alter cell fate decisions and may provide a new avenue for treating drug resistance.

Results

CRISPR–Cas9 genetic screens identify factors that affect primed cellular states. We wanted to identify factors that affected the fluctuations in cellular state that lead to single cells being primed to be drug resistant. We used a clonal $BRAF^{V600E}$-mutant melanoma cell line (WM989-A6-G3) that exhibits resistance behavior in cell culture[14] that is broadly comparable to that displayed in patients[14,21,26]. Phenomenologically, we observe that, upon addition of a roughly cytotoxic dose (1 μM) of the $BRAF^{V600E}$ inhibitor vemurafenib[14], the vast majority of cells die or stop growing, but around 1 in 2,000–3,000 cells continues to proliferate, ultimately forming a resistant colony after 2–3 weeks in culture in vemurafenib[14]. Before the application of drug, there is a rare subpopulation of cells that are primed to become resistant[14], and these cells are marked by the expression of a set of priming marker genes, like *NGFR* and *EGFR*. To identify modulators of the fluctuations that lead to the formation of this subpopulation of primed cells, we designed a loss-of-function pooled CRISPR genetic screen (dubbed the 'priming screen') composed of ~13,000 single guide RNAs (sgRNAs) targeting functionally relevant domains of ~2,000 proteins, with around six distinct sgRNAs per domain (1,402 transcription factor targets, 481 kinase targets and 176 epigenetic targets; Supplementary Tables 1–3)[27–29]. To conduct the screen, we stably integrated *Streptococcus pyogenes* Cas9 (spCas9) into the WM989-A6-G3 cell line, creating the clonal line WM989-A6-G3-Cas9-5a3 (Extended Data Figs. 1 and 2 show a comparison to the parental line and validation of spCas9 functionality).

To screen for factors affecting cellular priming, we transduced these cells with the pooled library of sgRNAs. To ensure adequate sampling of the frequency of rare primed cells, we expanded the culture to around 50,000–250,000 cells for each sgRNA, or roughly a billion cells in total. We combined magnetic sorting and flow cytometry to isolate cells expressing both EGFR and NGFR, which are well-validated markers of primed cells: sorting out cells expressing each marker produces far more resistant colonies, with double-positive cells being even more resistant[14,19]. (Note that these markers may not induce the primed state per se; indeed, inhibition of EGFR did not affect priming[14]). We sequenced the sgRNAs in this sorted subpopulation to determine which ones were over- or underrepresented compared to the unsorted population. Overrepresentation suggests that knockout of the gene increases the frequency of $NGFR^{HIGH}/EGFR^{HIGH}$ cells and vice versa (Fig. 1b). We selected 'hits' via a series of criteria that ranked candidates into confidence tiers (see Methods for selection criteria).

Our screen identified several factors that affect priming. We obtained a set of 61 high-confidence targets that affected the frequency of $NGFR^{HIGH}/EGFR^{HIGH}$ cells (Fig. 1c and Supplementary Table 4). Of these, 25 increased the frequency of $NGFR^{HIGH}/EGFR^{HIGH}$ cells and 36 decreased the frequency. Beyond known factors such as *SOX10* and *MITF*[26,30–32], we identified several factors not previously known to affect resistance to $BRAF^{V600E}$ inhibition. These include *DOT1L*, encoding an H3K79 methyltransferase associated with melanoma oncogenesis[33], and *BRD2*, a member of the BET family often overexpressed in melanoma[34]. In a secondary targeted screen of the 34 high-confidence targets, 25 replicated in the original WM989-A5-G3-Cas9 line and 20 showed similar effects in another melanoma line (451Lu-Cas9; Extended Data Fig. 3 and Supplementary Table 4). Together, these hits represented potential candidates for modulating priming and thus resistance. (Note that *EGFR* can be regarded as a positive control: our assay involved sorting for $EGFR^{HIGH}$ cells, so many genetic disruptions of *EGFR* would lead to a loss of EGFR protein).

Changes in drug resistance can occur by priming-dependent and -independent mechanisms. The priming screen was designed to identify candidate factors that would either increase or decrease the percentage of cells with a 'primed' transcriptional profile (high expression of *EGFR* and *NGFR*). Conceptually, a factor could also affect the number of resistant colonies without affecting priming, that is, without forcing cells to adopt the characteristic primed transcriptional profile. Instead, a factor could, say, increase the number of resistant colonies by lowering the priming 'threshold' needed for cells to become resistant, for instance, by lowering the level of residual mitogen-activated protein kinase signaling required for cells to proliferate in vemurafenib, allowing the survival of 'subprimed' cells that would normally not survive in drug. Thus, any particular factor could increase resistance by increasing the frequency of primed cells (Fig. 2a, middle) or by allowing more partially primed cells to become resistant (that is, lowering the putative threshold, Fig. 2a bottom), or both.

We wanted to measure how much these factors affected either priming frequency or resistance threshold. First, we ran a conventional survival screen (also, a secondary targeted screen with another melanoma line) based on the number of resistant colonies ('resistance screen'; Extended Data Figs. 3 and 4 and Supplementary Table 4). We identified 20 high-confidence factors that, when knocked out, increased the number of resistant cells, and 4 that reduced the number of resistant cells. The hits included signaling pathways elements like mitogen-activated protein kinase (*CSK*)[35], Wnt/β-catenin (*KDM2A*)[36] and Hippo (*LATS2*)[37].

It is important to note that neither the priming screen nor the resistance screen were run to saturation to identify all factors that affected either priming frequency or resistance threshold. Thus, even if a factor was identified in, say, the priming screen, it may also affect the number of resistant colonies even if it did not appear as a hit in the resistance screen (as discussed later). Therefore, the only way to systematically evaluate whether knocking out a factor would affect either priming frequency or resistance threshold (or both) was to measure, on a knockout-by-knockout basis, changes in the frequency of NGFR positivity and the number of resistant colonies produced, respectively. We measured NGFR positivity in 83 different targets taken from both screens, and further looked for changes in resistance in 35 of those (Fig. 2b and Extended Data Fig. 5). Individual knockouts exhibited a range of changes in both the frequency of $NGFR^{HIGH}$ cells and the number of resistant colonies formed. Many hits from the priming screen (15 of 21 tested by both immunofluorescence and resistant colony formation) showed the predicted change in the frequency of priming and, concomitantly, in the number of resistant colonies (for example, *LATS2* and *BRD2*; Fig. 2c), even over a range of drug concentrations (Extended Data Fig. 6a). Thus, knocking out factors that changed the frequency of cells expressing *NGFR* (a proxy for the primed cellular state) was associated with concordant changes in the number of resistant colonies.

It was possible that removal of a factor could increase the frequency of $NGFR^{HIGH}/EGFR^{HIGH}$ cells and the frequency of resistant colonies (Fig. 2c), but that the newly formed $NGFR^{HIGH}/EGFR^{HIGH}$ cells were not actually resistant and rather some other population was now responsible for the additional resistant colonies. To demonstrate that the newly formed $NGFR^{HIGH}/EGFR^{HIGH}$ cells were indeed driving the increased number of resistant colonies, we isolated $NGFR^{HIGH}/EGFR^{HIGH}$ cells from DOT1L-inhibited cells and added vemurafenib, and found that this now larger population of highly expressing cells had a similar if not higher propensity to become resistant; thus, the change in priming accounted for most of the resistant phenotype (Fig. 2e).

While there was an overall concordance between changes in priming and resistance, knockouts of many genes varied widely in the degree to which this relationship held (Fig. 2b). For instance, knockout of *EP300* increased NGFR^{HIGH} by ~twofold but only slightly increased the number of resistant colonies, while knockout of *CSK* only slightly increased the number of NGFR^{HIGH} cells but increased the number of resistant colonies over sixfold (Fig. 2b,c). Notably, knocking out *CSK* increased resistance to the point of producing a lawn of resistant cells, making it difficult to accurately count colonies and explaining why it was the dominant hit in the resistance screen. As mentioned, hits like *CSK* that affect resistance without affecting priming may affect the resistance threshold (Discussion).

Of the factors identified by the resistance screen, only five were also identified in our priming screen (Fig. 2d), suggesting that hits from the priming screen may not affect resistance. However, upon testing priming factors individually for their effects on the number of resistant colonies, most of the hits in the priming screen (15 of 21 tested) affected the number of resistant colonies (Extended Data Fig. 5b). This discordance highlights the utility of designing a screen focused on priming rather than resistance as a whole. In principle, if the resistance screen could isolate all possible factors affecting every aspect of resistance, then it would have found priming factors that also affect resistance. In practice, however, the number of cells required makes it difficult to run these screens to saturation, and as a result, dominant hits that change resistance alone (for example, *CSK*) comprised so many cells in the pooled resistance screen that priming factors became difficult to detect. Thus, screens targeting priming can potentially reveal new hits that may elude detection by other modes of screening.

Changes in the frequency of primed cellular states lead to in vivo tumor growth variability. We wondered whether the factors we identified could affect resistance in vivo, which has complex microenvironmental factors[38]. We tested three factors: *DOT1L* and *LATS2*, which increased the frequency of NGFR^{HIGH}/EGFR^{HIGH} cells in vitro, and *BRD2*, which decreased the frequency of these cells.

After knocking out these targets in WM989-A6-G3-Cas9-5a3 cells, we injected the cells into NOD/SCID (nonobese diabetic/severe combined immunodeficient) mice ($n=12$ mice per knockout) and allowed tumors to develop (Fig. 3). The tumor volumes over time were consistent with our in vitro results: at the treatment endpoint (Methods), *DOT1L* knockout tumors treated with a BRAF^{V600E} inhibitor were roughly 3.5 times larger than controls ($P=0.010$), and *LATS2* knockout tumors were 1.6 times larger than controls ($P=0.062$). Meanwhile, *BRD2*-knockout tumors were approximately half as big as controls ($P=0.045$). In the absence of drug, both knockout and control melanoma cells showed roughly similar growth dynamics (Fig. 3, bottom). Thus, priming factors also affect the response of tumors to BRAF^{V600E} inhibition in vivo.

Relative timing of targeting variability can affect drug resistance. Priming factors may affect resistance through mechanisms that can interact with BRAF^{V600E} inhibition in previously uncharacterized ways. For instance, a factor could affect the number of primed cells before BRAF^{V600E} inhibition but not after, once the cells begin reprogramming toward stable resistance. Inhibiting such a factor before inhibiting BRAF^{V600E} would be critical.

To test this possibility, we used the DOT1L inhibitor pinostat[39,40], which increases the number of colonies resistant to BRAF^{V600E} and MEK inhibitors (Extended Data Fig. 7a–c), to see if the relative timing of DOT1L inhibition affected the formation of resistant colonies. In addition to vemurafenib treatment, we pretreated cells with the DOT1L inhibitor for 7 d and co-treated with the DOT1L inhibitor concurrently with vemurafenib (Fig. 4a). Pre-inhibition of DOT1L resulted in threefold more colonies, but co-treatment led to no change in the number of resistant colonies (Fig. 4b). Thus, the relative timing of inhibition of cellular priming vis-à-vis mainline therapy can have a profound effect on resistance.

Knockout of genes that increase the frequency of primed cell states also increase cellular differentiation. Our priming screens identified factors that operate via a variety of signaling pathways and transcriptional regulatory mechanisms. Interestingly, a priori, no particular pathway dominated the set of identified factors; however, seemingly unrelated genes nevertheless could affect priming through common biological processes.

Fig. 2 | Effects of modulators of cellular priming on resistant colony formation. a, In melanoma, the frequency of primed cells in the population dictates the degree of resistance to BRAF^{V600E} inhibition. Changes to the mapping between cellular priming and the response of a cell to the drug can alter the number of resistant colonies that form upon addition of the BRAF^{V600E} inhibitor vemurafenib. **b**, Relationship between the frequency of NGFR^{HIGH} cells (*x* axis) and the number of resistant colonies (*y* axis). We plotted the frequency of NGFR^{HIGH} cells as the mean $\log_2$ fold change over three replicates in the number of NGFR^{HIGH} cells following knockout of the gene indicated, normalized by cells with nontargeting sgRNAs (for variability of the effect size across replicates of a given target, see Extended Data Fig. 5). We quantified the $\log_2$ fold change in the number of resistant colonies in the knockout cell line as compared to the nontargeting control cell lines. Orange points are targets identified as high-confidence hits (tier 1 and tier 2) in the cellular priming screen; blue are those identified as high-confidence hits in the resistance screen; purple are those identified as high-confidence hits in both screens; gray are those that may have shown an effect in either or both screens but were not classified as high-confidence hits in either screen. **c**, To validate the phenotypic effect of targets identified by our genetic screens, we knocked out 83 of the targets and quantified both the frequency of NGFR^{HIGH} cells by immunofluorescence using anti-NGFR antibodies (top) and the number of resistant colonies (bottom) that formed upon BRAF^{V600E} inhibition. Here we show example validation of *BRD2* and *LATS2* knockouts (hits in the cellular priming screen) and of *CSK* knockouts (hit in the resistance screen only). The schematic represents the effect of the knockout in the priming screen on the frequency of NGFR^{HIGH}/EGFR^{HIGH} cells. The immunofluorescence data was captured in three biological replicates. The colony formation assays for this specific experiment were carried out once (Extended Data Fig. 5a,b). Of note, the number of colonies reported for the *CSK* knockout is an underestimate due to difficulties in accurately counting colonies in highly confluent plates. **d**, Effect overlap between hits from the cellular priming and resistance screens. The position of each target (dots) represents the number of times (as median $\log_2$ fold change) the sgRNAs were detected in the NGFR^{HIGH}/EGFR^{HIGH} population versus an unsorted population of melanoma cells (priming screen; *x* axis) or in the population of cells resistant to vemurafenib versus the population of cells before treatment (resistance screen; *y* axis). Orange labels correspond to high-confidence targets (tier 1 and tier 2) in the cellular priming screen; blue corresponds to high-confidence targets in the resistance screen; purple corresponds to high-confidence targets in both screens. The effects of all targets in both screens are displayed as a density histogram. **e**, To compare the resistance potential of primed cells (marked by NGFR and EGFR expression) resulting from inhibition of DOT1L (a target from the priming screen) with that of control populations, we first pretreated cells with either a DOT1L inhibitor (EPZ5676) or DMSO for 7 d. We then sorted cells by NGFR and EGFR expression using FACS. Then, we treated an equal number of cells with vemurafenib and quantified the resulting number of drug-resistant colonies. Dots represent individual data points. The bars represent the average number of colonies in each population across triplicates, normalized to every 1,000 cells present before addition of vemurafenib. Error bars represent the standard deviation across triplicates.

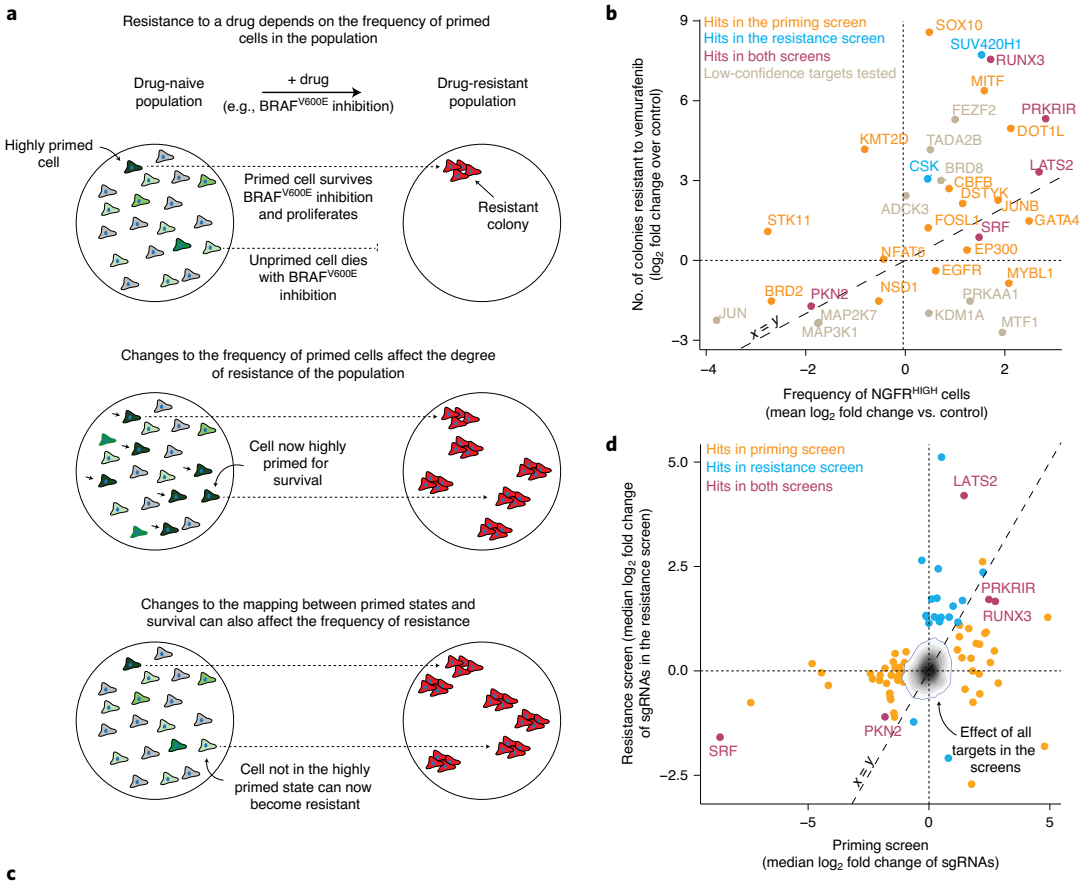
a
Resistance to a drug depends on the frequency of primed cells in the population
Drug-naive population
+ drug
(e.g., BRAF^{V600E} inhibition)
Drug-resistant population
Highly primed cell
Primed cell survives BRAF^{V600E} inhibition and proliferates
Resistant colony
Unprimed cell dies with BRAF^{V600E} inhibition
Changes to the frequency of primed cells affect the degree of resistance of the population
Cell now highly primed for survival
Changes to the mapping between primed states and survival can also affect the frequency of resistance
Cell not in the highly primed state can now become resistant
b
Hits in the priming screen
Hits in the resistance screen
Hits in both screens
Low-confidence targets tested
No. of colonies resistant to vemurafenib (log2 fold change over control)
Frequency of NGFR^{HIGH} cells (mean log2 fold change vs. control)
SOX10
SUV420H1
RUNX3
MITF
FEZF2
PRKRIR
DOT1L
KMT2D
TADA2B
CSK
BRD8
LATS2
CBFB
DSTYK
ADCK3
JUNB
STK11
FOSL1
GATA4
SRF
NFAT5
EP300
EGFR
MYBL1
BRD2
PKN2
NSD1
PRKAA1
JUN
MAP2K7
KDM1A
MTF1
MAP3K1
d
Hits in priming screen
Hits in resistance screen
Hits in both screens
Resistance screen (median log2 fold change of sgRNAs in the resistance screen)
Priming screen (median log2 fold change of sgRNAs)
LATS2
PRKRIR
RUNX3
PKN2
SRF
Effect of all targets in the screens
c
Effect in the priming screen
Negative control
BRD2 knockout
DOT1L knockout
LATS2 knockout
CSK knockout
DAPI
NGFR IF
NGFR^{HIGH} cell
500 µm
Colony formation assay
Resistant colony
10 mm
Coalesced resistant colonies
e
DMSO pretreated cells
EGFR expression (EGFR-cy3 signal intensity)
NGFR expression (NGFR-APC signal intensity)
All cells
2.91%
NGFR^{HIGH}/EGFR^{HIGH}
1.08%
NGFR^{LOW}/EGFR^{LOW}
Treat equal no. of cells with PLX4032
+PLX4032
EPZ5676 pretreated cells
4.34%
1.68%
No. of resistant colonies (per every 1,000 cells alive before vemurafenib therapy)
All cells
NGFR^{HIGH}/EGFR^{HIGH}
NGFR^{LOW}/EGFR^{LOW}

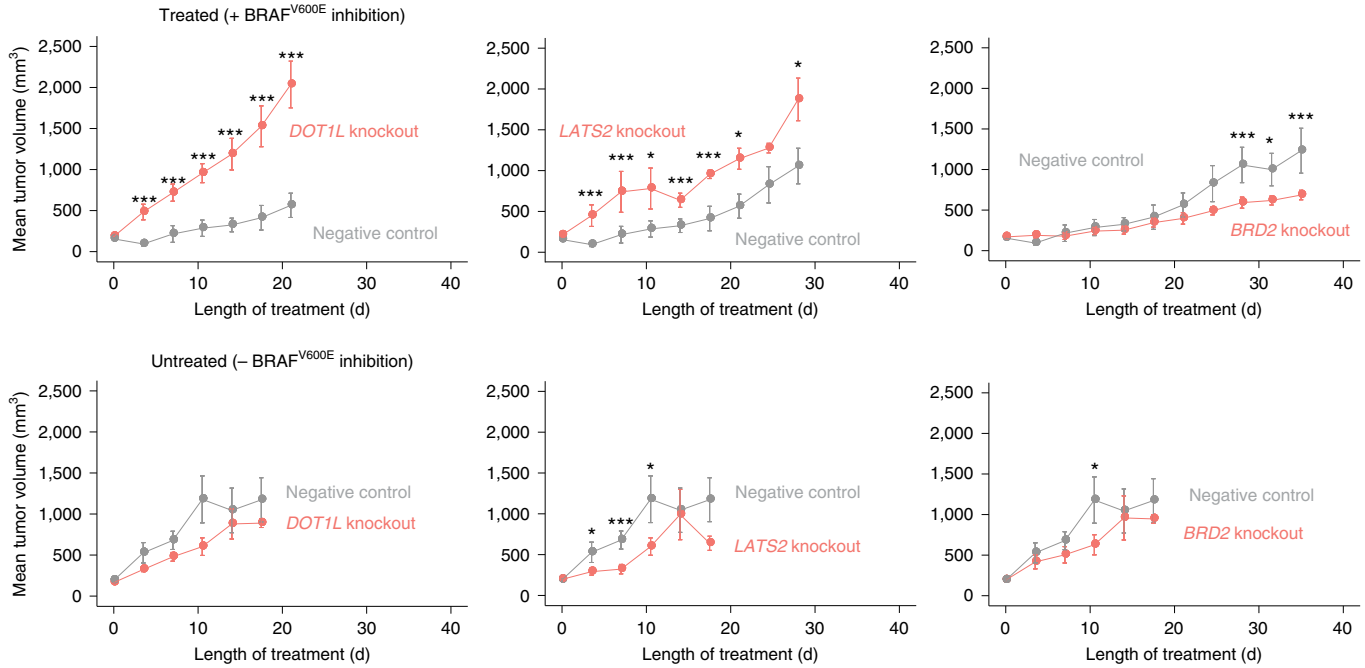

Fig. 3 | Effect of modulators of cellular priming on growth of BRAF^{V600E}-resistant tumors in vivo. Tumor volume as a function of time in xenografts (NOD/SCID mice) treated with a BRAF^{V600E} inhibitor (top) or vehicle control (bottom). Here, we injected each mouse with *DOT1L*-, *LATS2*- or *BRD2*-knockout WM989-A6-G3-Cas9 cells (orange) or the same cell line without a gene knockout (gray). The values plotted represent the mean tumor volume across mice carrying the same knockout. Error bars represent the standard error of the mean. All *P* values were obtained with a one-sided *t*-test. The asterisks mark time points at which the difference in tumor volume between knockout and control groups reached significance (***$P \leq 0.05$ and *$P = 0.1 \leq \geq 0.05$; Methods). Each group started with $n = 6$ mice, and we plotted the mean tumor volume up until both knockout and negative control groups had at least $n = 3$ mice each. The *n* at each time point and their respective *P* values are presented in Supplementary Tables 7 and 8.

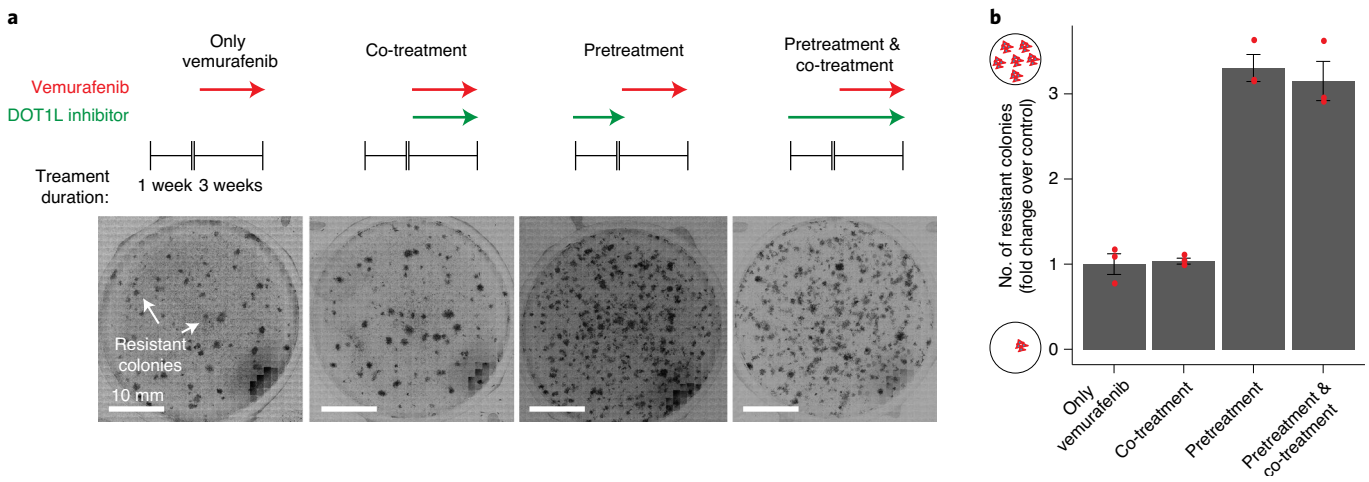

Fig. 4 | Effect of targeting cellular priming at different times relative to BRAF^{V600E} inhibition. a, To assess the effect of DOT1L inhibition (green arrows; 4 μM pinometostat) at different times on a cell's ability to survive BRAF^{V600E} inhibition, we first established a baseline number of colonies that grow when WM989-A6-G3 cells are exposed to 1 μM of vemurafenib for 3 weeks (leftmost panel). Then, in a separate population, we inhibited BRAF^{V600E} and DOT1L simultaneously (co-treatment), inhibited DOT1L first (7 d) and then BRAF^{V600E} (3 additional weeks; pretreatment) or inhibited DOT1L before (7 d) and during 3 weeks of vemurafenib treatment (pretreatment and co-treatment). **b**, Number of resistant colonies resulting from each therapeutic regimen in Fig. 4a as the fold change versus baseline (vemurafenib alone) for three replicates normalized to the number of cells in culture before BRAF^{V600E} inhibition. Dots represent individual data points. The bars quantify the mean fold change across the three replicates. Error bars indicate the standard error.

To look for such commonalities, we used RNA sequencing to measure genome-wide transcript levels for 266 knockout cell lines targeting 80 different proteins taken from both the priming and resistance screens (see Supplementary Table 4 and Extended Data Figs. 8 and 9 for information regarding validation rates of the targets used), reasoning that genes participating in a particular biological process may exhibit similar patterns of differential expression when knocked out.

Clustering the transcriptome profiles from the different knockout cell lines (Extended Data Fig. 10a) showed that, while the

transcriptomes induced by some gene knockouts were clearly distinct (such as *MITF*, *SOX10* and *KDM1A*), many others appeared to show only relatively small differences from the parental cell line. We reasoned that, while the sets of differentially expressed genes may be nonoverlapping, they could still belong to the same pathway. Using the transcriptome of each knockout, we performed a gene-set enrichment analysis (GSEA; Methods) and obtained an enrichment score for biological processes from the Gene Ontology (GO) terms database (Fig. 5a)[41]. Using these enrichment scores, the knockout lines clustered in a more coherent pattern. Notable associations include cluster 5, containing the canonical melanocyte master regulators *MITF* and *SOX10*, and cluster 1, containing *DOT1L*, *LATS2*, *RUNX3* and *GATA4*.

Interestingly, knocking out *MITF* and *SOX10* increased drug resistance, as did knocking out most members of cluster 1, but the transcriptome profiles of these two clusters appeared to be roughly opposite of each other. The GO gene sets in group E, which appeared maximally different between MITF/SOX10 and cluster 1, included several related to differentiation, including sets for melanocyte differentiation and neural crest differentiation (Fig. 5b). Knockout of *MITF* and *SOX10* decreased the expression of these genes, matching the general consensus that drug resistance is typically driven by dedifferentiation[8,26]. It was thus unexpected that most elements of cluster 1 increased resistance by further promoting differentiation (Fig. 5c), suggesting a possible new mechanism by which one could affect drug resistance; the latter has further support from the importance of timing in DOT1L inhibition (Fig. 4). This axis of differentiation was coordinated across several gene sets (Extended Data Fig. 10b). (Note that the role of *MITF* in therapy resistance is complex in general[42]).

The knockout of targets that led to differentiation and dedifferentiation had characteristic changes in priming and resistance. Knockouts in cluster 1 (differentiation) mimicked many aspects of the transcriptomes of NGFR^{HIGH}, EGFR^{HIGH}, NGFR^{HIGH}/EGFR^{HIGH} and even vemurafenib-resistant melanoma cells (expression of genes involved in cell–matrix adhesion, angiogenesis and cell migration; Fig. 5a,b). Knockouts of these targets showed a strong and often proportional correspondence between the frequency of NGFR^{HIGH} cells and the number of colonies that developed under BRAF inhibition, suggesting that the increase/decrease in the frequency of primed cells was the cause of increased/decreased resistance (Fig. 5d; for example, *LATS2*, *JUNB*, *FOSL1* and *CBFB*). For *MITF* and *SOX10* (cluster 5), however, the frequency of NGFR^{HIGH} cells did not change nearly as much as the number of resistant colonies.

Different categories of knockouts resulted in a reduction (as opposed to increase) in the number of resistant colonies. Some resistance-reducing knockouts (*BRD8* and *PRKAA1*) clustered with *DOT1L*, while another (*BRD2)* clustered with *MITF/SOX10*. It is possible that these factors work in inverse ways to reduce drug resistance by either affecting differentiation or dedifferentiation. Meanwhile, the majority of resistance-reducing knockouts appeared to cluster separately. Cluster 2 was associated with metabolism (for example, biosynthesis of amino acids and acyl-CoA metabolism), suggesting that metabolic processes may reduce drug resistance (Supplementary Table 6). The other clusters did not show any coherent set of biological processes affected (for example, *SRC*, *IRF7* and *PKN2*, among others).

We also wanted to check what inhibiting these factors did to the transcriptomes of the NGFR^{HIGH}/EGFR^{HIGH} cells specifically. We isolated NGFR^{HIGH}/EGFR^{HIGH} cells both from WM989-A6-G3 cells pretreated with a DOT1L inhibitor (pinometostat) and from WM989-A6-G3 cells pretreated with dimethylsulfoxide (DMSO) and then measured the transcriptomes of these subpopulations. A principal-component analysis of these transcriptomes showed that DOT1L inhibition led to newly primed cells that were transcriptionally similar to the primed cells in the DMSO-treated population (extensively explored and described by Shaffer et al.[14]), suggesting that the changes we induced indeed led to new primed cells that are transcriptomically similar to those in non-DOT1L-inhibited cells (Fig. 5e,f).

Discussion

We have demonstrated, using high-throughput genetic screening, that there are genetic factors that can alter cellular plasticity in cancer cells, thereby affecting their resistance to targeted therapeutics. These factors revealed new vulnerabilities beyond conventional genetic screens, demonstrating the potential of screens designed

Fig. 5 | Gene-set enrichment analysis of the transcriptional effects induced by knockout of select screen targets. a, The heat map represents biclustering analysis of different knockout cell lines (rows) based on the GSEA score of GO gene sets. Within the heat map, red indicates enrichment in the sense that there are more differentially upregulated genes in knockout versus control in that gene set than expected by chance, whereas blue indicates enrichment of downregulated genes (shade indicates degree of enrichment). Each target knockout (rows) represents transcriptomes of biological triplicates (unless otherwise stated in Supplementary Table 4). Target labels (rows) in green indicate genes whose knockout increased the frequency of NGFR^{HIGH}/EGFR^{HIGH} cells in the screen, while red indicates targets whose knockout increased the number of cells resistant to vemurafenib, and gray indicates targets that decreased the frequency of either NGFR^{HIGH}/EGFR^{HIGH} cells or cells resistant to vemurafenib. As before, we organized targets into high-confidence hits (tiers 1 and 2) and low-confidence hits (tiers 3 and 4) based on the percentage of sgRNAs against a target that showed at least a twofold change in the initial screen (see 'knockout color key'). The asterisks next to the label indicate the tier (tier 1, ****; tier 2, ***; tier 3, **; tier 4, *). Information regarding validation rates of each tier can be found in Extended Data Figs. 8 and 9. Based on the dendrogram (left), we grouped targets into six clusters. We also clustered gene sets (columns) into groups, labeled by the letters on top of the heat map. The white boxes inside the heat map demark groups of gene sets specifically upregulated in a given cluster. **b**, Select list of gene sets in groups D and E from **a** (for a complete list of gene sets within each group, see Supplementary Table 6). **c**, Relationship between the expression of genes involved in neural crest differentiation (*x* axis) and the number of colonies resistant to vemurafenib (*y* axis) following the knockout of a target. For each knockout, we plotted the expression of neural crest differentiation genes as the enrichment score obtained through GSEA for the neural crest differentiation gene set (GO term). We quantified the $\log_2$ (fold change) in the number of resistant colonies in the knockout cell line as compared to the nontargeting control cell lines. Colors represent the cluster grouping of each knockout based on **a**. **d**, Relationship between the frequency of NGFR^{HIGH} cells (*x* axis) and the number of resistant colonies (*y* axis). We plotted the frequency of NGFR^{HIGH} cells as the median $\log_2$ (fold change) over three replicates in the number of NGFR^{HIGH} cells following knockout of the indicated gene normalized by cells with nontargeting sgRNAs (for variability of the effect size across replicates of a given target, see Extended Data Fig. 5.) We quantified the $\log_2$ (fold change) in the number of resistant colonies in the knockout cell line as compared to the nontargeting control cell lines. We color coded all targets by groupings based on their transcriptomes (see **a**) following knockout of the gene indicated. **e**,**f**, We performed principal-component analysis of the transcriptome of different subpopulations of primed and unprimed cells in either control melanoma populations or cells where we inhibited DOT1L. We used as input the gene expression levels of all expressed genes (normalized to reads per million) to identify primary axes that accounted for the greatest degree of transcriptome variability between these populations of cells. In **e**, the color indicates the phenotype of the population, meaning a mixture of all the melanoma cells (gray), only cells expressing NGFR and EGFR (green) or only cells with low levels of NGFR and EGFR (brown). In **f**, the color indicates whether the cells were pretreated with the DOT1L inhibitor EPZ5676 (blue) or with DMSO (pink).

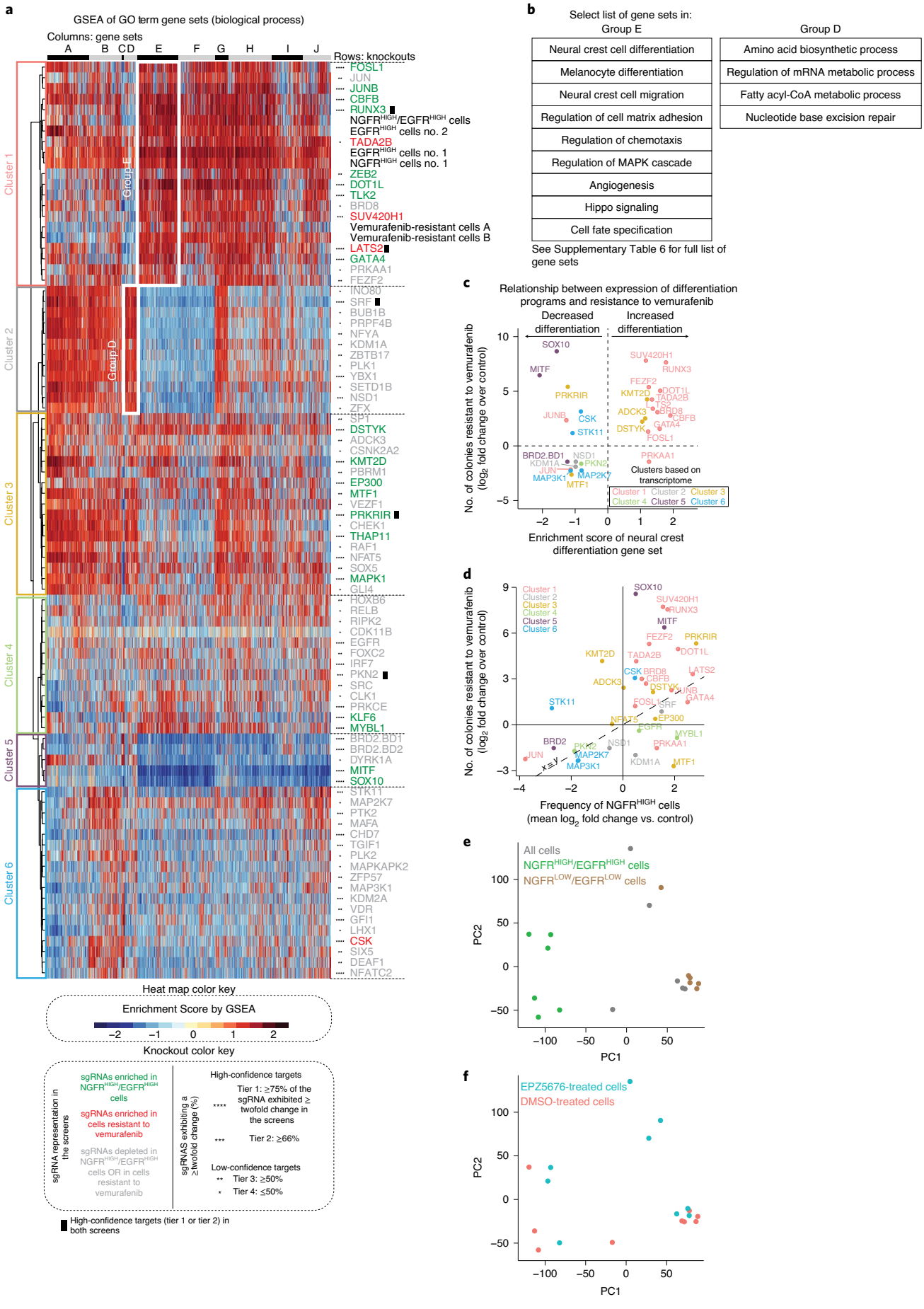
a
GSEA of GO term gene sets (biological process)
Columns: gene sets
A B CD E F G H I J
Rows: knockouts
Cluster 1
Cluster 2
Cluster 3
Cluster 4
Cluster 5
Cluster 6
Group E
Group D
FOSL1
JUN
JUNB
CBFB
RUNX3
NGFR^HIGH/EGFR^HIGH cells
EGFR^HIGH cells no. 2
TADA2B
EGFR^HIGH cells no. 1
NGFR^HIGH cells no. 1
ZEB2
DOT1L
TLK2
BRD8
SUV420H1
Vemurafenib-resistant cells A
Vemurafenib-resistant cells B
LATS2
GATA4
PRKAA1
FEZF2
INO80
SRF
BUB1B
PRPF4B
NFYA
KDM1A
ZBTB17
PLK1
YBX1
SETD1B
NSD1
ZFX
SP1
DSTYK
ADCK3
CSNK2A2
KMT2D
PBRM1
EP300
MTF1
VEZF1
PRKRIR
CHEK1
THAP11
RAF1
NFAT5
SOX5
MAPK1
GLI4
HOXB6
RELB
RIPK2
CDK11B
EGFR
FOXC2
IRF7
PKN2
SRC
CLK1
PRKCE
KLF6
MYBL1
BRD2.BD1
BRD2.BD2
DYRK1A
MITF
SOX10
STK11
MAP2K7
PTK2
MAFA
CHD7
TGIF1
PLK2
MAPKAPK2
ZFP57
MAP3K1
KDM2A
VDR
GFI1
LHX1
CSK
SIX5
DEAF1
NFATC2
Heat map color key
Enrichment Score by GSEA
−2 −1 0 1 2
Knockout color key
sgRNA representation in the screens
sgRNAs enriched in NGFR^HIGH/EGFR^HIGH cells
sgRNAs enriched in cells resistant to vemurafenib
sgRNAs depleted in NGFR^HIGH/EGFR^HIGH cells OR in cells resistant to vemurafenib
sgRNAS exhibiting a ≥twofold change (%)
High-confidence targets
**** Tier 1: ≥75% of the sgRNA exhibited ≥ twofold change in the screens
*** Tier 2: ≥66%
Low-confidence targets
** Tier 3: ≥50%
* Tier 4: ≤50%
High-confidence targets (tier 1 or tier 2) in both screens
b
Select list of gene sets in:
Group E
Neural crest cell differentiation
Melanocyte differentiation
Neural crest cell migration
Regulation of cell matrix adhesion
Regulation of chemotaxis
Regulation of MAPK cascade
Angiogenesis
Hippo signaling
Cell fate specification
Group D
Amino acid biosynthetic process
Regulation of mRNA metabolic process
Fatty acyl-CoA metabolic process
Nucleotide base excision repair
See Supplementary Table 6 for full list of gene sets
c
Relationship between expression of differentiation programs and resistance to vemurafenib
Decreased differentiation
Increased differentiation
No. of colonies resistant to vemurafenib (log2 fold change over control)
Enrichment score of neural crest differentiation gene set
Clusters based on transcriptome
Cluster 1 Cluster 2 Cluster 3
Cluster 4 Cluster 5 Cluster 6
d
No. of colonies resistant to vemurafenib (log2 fold change over control)
Frequency of NGFR^HIGH cells (mean log2 fold change vs. control)
e
All cells
NGFR^HIGH/EGFR^HIGH cells
NGFR^LOW/EGFR^LOW cells
PC1
PC2
f
EPZ5676-treated cells
DMSO-treated cells
PC1
PC2

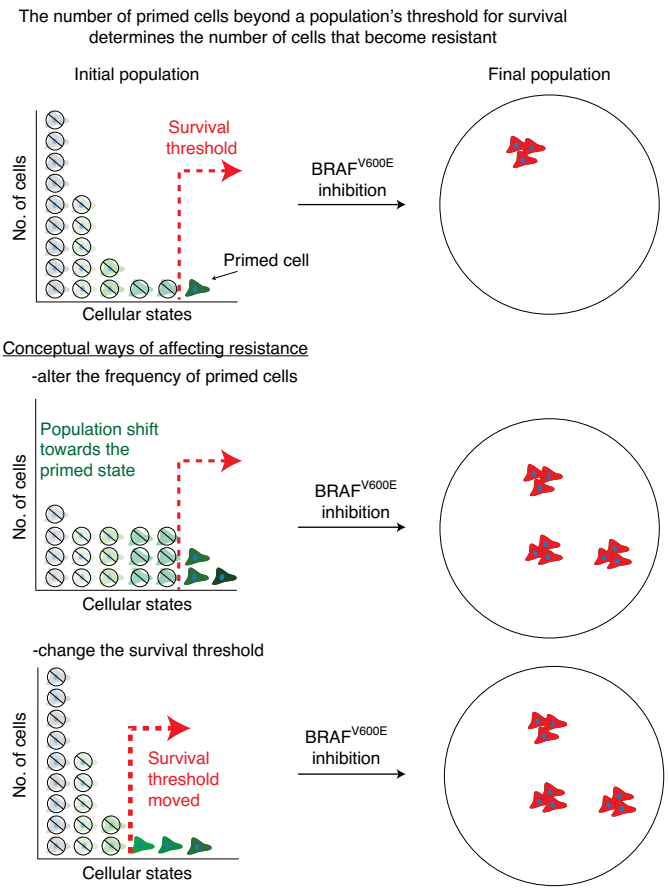

Fig. 6 | Model of survival threshold and cellular priming in the development of resistance to targeted therapies. Variability in the expression of various markers is associated with an individual cell's probability to survive drug treatment. In one simple model, cellular variability occurs along a single ordinate, which can be conceptualized as the degree of 'greenness'. In this model, there is a threshold (red dashed line, top panel) that divides cells along this axis into those that adapt to the drug and become resistant versus those that no longer proliferate when challenged with drug. Here, there are at least two ways by which one could conceivably alter the number of cells that survive the drug. In one scenario (middle), the distribution of 'greenness' could change, resulting in more cells being above the threshold, leading to more resistant colonies. In another scenario, the distribution of phenotypes remains unchanged, but the threshold itself moves, also leading to more resistant colonies. Our results suggest (but do not prove) that both scenarios may play out to varying degrees as a result of different genes being knocked out.

to target cellular priming. Drug screens targeting gene expression 'noise' have also shown similar therapeutic potential[43].

Some priming factors (*SOX10* and *MITF*) play critical roles in differentiation and drug resistance[26,30–32], while others (*LATS2* and *RUNX3*) are involved in 'stemness' and drug resistance[37,44,45]. Note, however, that no single factor or pathway dominated, that is, there was no 'smoking gun'. This may be because our screen did not target all potential regulators. Alternatively, it may be that the biology of cellular variability is intrinsically multifactorial[15].

The technical challenges associated with performing rare-cell screens at full depth provide motivation to screen for priming. In principle, a resistance screen would reveal all factors affecting resistance, including those that affect priming, but there was relatively little overlap between our priming and resistance screens. The fact that the majority of the genes identified in our priming screen did in fact affect resistance when tested individually suggests that they may have been identified were it possible to run resistance screens to saturation.

Knocking out some factors led to discordant changes in the frequencies of NGFR^{HIGH} cells and resistant colonies. The former may primarily affect cellular priming, that is, the cellular state, while the latter may affect the mapping between initial cellular states and their fates upon the addition of vemurafenib. (Here, the 'mapping' refers to the connections between states like 'AXL^{HIGH}' and fates like 'drug resistant' or 'drug sensitive'). In one simple model, cells occupy a distribution of states, and those above a threshold survive drug and those below do not (Fig. 6). In this model, some knockouts may alter the distribution of cells in the initial population or the threshold itself, or some combination of both. It is wise to caution against this simple interpretation, however. *NGFR* expression is just a marker for the primed state, and factors may affect the frequency of primed cells without showing any effect on *NGFR* expression. An argument against this is the fact that the transcriptomes of knockouts such as *DOT1L* that increase the frequency of NGFR and resistance appear to be similar to the profile of NGFR^{HIGH} cells themselves (Fig. 5a). It is also likely that a number of different types of resistant cells exist; anecdotally, we have noticed that resistant cells from some of our knockout lines do appear morphologically different. Such results suggest a mapping from a continuum of initial cellular states to multiple cellular fates.

We have observed similar rare-cell variability in primary melanocytes[14], raising the possibility that the same variability may also play a role in normal biological processes. The factors we have isolated may play a role in regulating variability in these normal biological contexts. Uncovering the regulators of the mapping between variable cellular states and ultimate phenotypic fates may prove fruitful, both conceptually and practically.

Online content

Any methods, additional references, Nature Research reporting summaries, source data, extended data, supplementary information, acknowledgements, peer review information; details of author contributions and competing interests; and statements of data and code availability are available at https://doi.org/10.1038/s41588-020-00749-z.

Received: 22 September 2019; Accepted: 12 November 2020;
Published online: 4 January 2021

References

1. Symmons, O. & Raj, A. What's luck got to do with it: single cells, multiple fates and biological nondeterminism. *Mol. Cell* **62**, 788–802 (2016).
2. Raj, A. & van Oudenaarden, A. Nature, nurture or chance: stochastic gene expression and its consequences. *Cell* **135**, 216–226 (2008).
3. Raj, A., Rifkin, S. A., Andersen, E. & van Oudenaarden, A. Variability in gene expression underlies incomplete penetrance. *Nature* **463**, 913–918 (2010).
4. Wernet, M. F. et al. Stochastic spineless expression creates the retinal mosaic for colour vision. *Nature* **440**, 174–180 (2006).
5. Süel, G. M., Kulkarni, R. P., Dworkin, J., Garcia-Ojalvo, J. & Elowitz, M. B. Tunability and noise dependence in differentiation dynamics. *Science* **315**, 1716–1719 (2007).
6. Maamar, H., Raj, A. & Dubnau, D. Noise in gene expression determines cell fate in *Bacillus subtilis*. *Science* **317**, 526–529 (2007).
7. Mojtahedi, M. et al. Cell fate decision as high-dimensional critical state transition. *PLoS Biol.* **14**, e2000640 (2016).
8. Rambow, F. et al. Toward minimal residual disease-directed therapy in melanoma. *Cell* **174**, 843–855 (2018).
9. Garraway, L. A. & Jänne, P. A. Circumventing cancer drug resistance in the era of personalized medicine. *Cancer Discov.* **2**, 214–226 (2012).
10. Trunzer, K. et al. Pharmacodynamic effects and mechanisms of resistance to vemurafenib in patients with metastatic melanoma. *J. Clin. Oncol.* **31**, 1767–1774 (2013).
11. Sharma, S. V. et al. A chromatin-mediated reversible drug-tolerant state in cancer cell subpopulations. *Cell* **141**, 69–80 (2010).
12. Gupta, P. B. et al. Stochastic state transitions give rise to phenotypic equilibrium in populations of cancer cells. *Cell* **146**, 633–644 (2011).

13. Pisco, A. O. & Huang, S. Nongenetic cancer cell plasticity and therapy-induced stemness in tumour relapse: 'What does not kill me strengthens me'. *Br. J. Cancer* **112**, 1725–1732 (2015).
14. Shaffer, S. M. et al. Rare-cell variability and drug-induced reprogramming as a mode of cancer drug resistance. *Nature* **546**, 431–435 (2017).
15. Shaffer, S. M. et al. Memory sequencing reveals heritable single-cell gene expression programs associated with distinct cellular behaviors. *Cell* **182**, 947–959 (2020).
16. Cohen, A. A. et al. Dynamic proteomics of individual cancer cells in response to a drug. *Science* **322**, 1511–1516 (2008).
17. Weinreb, C., Rodriguez-Fraticelli, A., Camargo, F. D. & Klein, A. M. Lineage tracing on transcriptional landscapes links state to fate during differentiation. *Science* **367**, eaaw3381 (2020).
18. Su, Y. et al. Single-cell analysis resolves the cell state transition and signaling dynamics associated with melanoma drug-induced resistance. *Proc. Natl Acad. Sci. USA* **114**, 13679–13684 (2017).
19. Fallahi-Sichani, M. et al. Adaptive resistance of melanoma cells to RAF inhibition via reversible induction of a slowly dividing dedifferentiated state. *Mol. Syst. Biol.* **13**, 905 (2017).
20. Torre, E. et al. Rare-cell detection by single-cell RNA sequencing as guided by single-molecule RNA FISH. *Cell Syst.* **6**, 171–179 (2018).
21. Tirosh, I. et al. Dissecting the multicellular ecosystem of metastatic melanoma by single-cell RNA-seq. *Science* **352**, 189–196 (2016).
22. Shalem, O. et al. Genome-scale CRISPR–Cas9 knockout screening in human cells. *Science* **343**, 84–87 (2014).
23. Konermann, S. et al. Genome-scale transcriptional activation by an engineered CRISPR–Cas9 complex. *Nature* **517**, 583–588 (2015).
24. Strub, T. et al. SIRT6 haploinsufficiency induces $BRAF^{V600E}$ melanoma cell resistance to MAPK inhibitors via IGF signalling. *Nat. Commun.* **9**, 3440 (2018).
25. Joung, J. et al. Genome-scale activation screen identifies a lncRNA locus regulating a gene neighbourhood. *Nature* **548**, 343–346 (2017).
26. Sun, C. et al. Reversible and adaptive resistance to BRAF(V600E) inhibition in melanoma. *Nature* **508**, 118–122 (2014).
27. Huang, Y.-H. et al. POU2F3 is a master regulator of a tuft cell-like variant of small cell lung cancer. *Genes Dev.* **32**, 915–928 (2018).
28. Tarumoto, Y. et al. LKB1, salt-inducible kinases, and MEF2C are linked dependencies in acute myeloid leukemia. *Mol. Cell* **69**, 1017–1027 (2018).
29. Brien, G. L. et al. Targeted degradation of BRD9 reverses oncogenic gene expression in synovial sarcoma. *eLife* **7**, e41305 (2018).
30. Almeida, F. V., Douglass, S. M., Fane, M. E. & Weeraratna, A. T. Bad company: microenvironmentally mediated resistance to targeted therapy in melanoma. *Pigment Cell Melanoma Res.* **32**, 237–247 (2019).
31. Hartman, M. L. & Czyz, M. MITF in melanoma: mechanisms behind its expression and activity. *Cell. Mol. Life Sci.* **72**, 1249–1260 (2015).
32. Wellbrock, C. & Arozarena, I. Microphthalmia-associated transcription factor in melanoma development and MAP-kinase pathway targeted therapy. *Pigment Cell Melanoma Res.* **28**, 390–406 (2015).
33. Zhu, B. et al. The protective role of DOT1L in UV-induced melanomagenesis. *Nat. Commun.* **9**, 259 (2018).
34. Segura, M. F. et al. BRD4 sustains melanoma proliferation and represents a new target for epigenetic therapy. *Cancer Res.* **73**, 6264–6276 (2013).
35. Okada, M., Nada, S., Yamanashi, Y., Yamamoto, T. & Nakagawa, H. CSK: a protein-tyrosine kinase involved in regulation of src family kinases. *J. Biol. Chem.* **266**, 24249–24252 (1991).
36. Lu, L. et al. Kdm2a/b lysine demethylases regulate canonical Wnt signaling by modulating the stability of nuclear β-catenin. *Dev. Cell* **33**, 660–674 (2015).
37. Harvey, K. F., Zhang, X. & Thomas, D. M. The Hippo pathway and human cancer. *Nat. Rev. Cancer* **13**, 246–257 (2013).
38. Kaur, A. et al. sFRP2 in the aged microenvironment drives melanoma metastasis and therapy resistance. *Nature* **532**, 250–254 (2016).
39. Daigle, S. R. et al. Selective killing of mixed lineage leukemia cells by a potent small-molecule DOT1L inhibitor. *Cancer Cell* **20**, 53–65 (2011).
40. Basavapathruni, A. et al. Conformational adaptation drives potent, selective and durable inhibition of the human protein methyltransferase DOT1L. *Chem. Biol. Drug Des.* **80**, 971–980 (2012).
41. Subramanian, A. et al. Gene-set enrichment analysis: a knowledge-based approach for interpreting genome-wide expression profiles. *Proc. Natl Acad. Sci. USA* **102**, 15545–15550 (2005).
42. Bai, X., Fisher, D. E. & Flaherty, K. T. Cell-state dynamics and therapeutic resistance in melanoma from the perspective of MITF and IFNγ pathways. *Nat. Rev. Clin. Oncol.* **16**, 549–562 (2019).
43. Dar, R. D., Hosmane, N. N., Arkin, M. R., Siliciano, R. F. & Weinberger, L. S. Screening for noise in gene expression identifies drug synergies. *Science* **344**, 1392–1396 (2014).
44. Aylon, Y., Sarver, A., Tovy, A., Ainbinder, E. & Oren, M. Lats2 is critical for the pluripotency and proper differentiation of stem cells. *Cell Death Differ.* **21**, 624–633 (2014).
45. Kulkarni, M. et al. RUNX1 and RUNX3 protect against YAP-mediated EMT, stem-ness and shorter survival outcomes in breast cancer. *Oncotarget* **9**, 14175–14192 (2018).

Methods

Cell culture. We obtained patient-derived melanoma cells (WM989 and 451Lu, female and male, respectively) from the laboratory of M. Herlyn. Both the WM989 and the 451Lu cell lines contain the p.Val600Glu-encoding mutation at codon 600 in the *BRAF* gene. This mutation causes constitutively active kinase activity and activation of the MEK and ERK signaling pathway. The WM989 cell line expresses wild-type N-RAS, c-KIT and CDK4, and 451Lu is wild-type for PTEN, N-RAS, c-KIT and CDK4. For WM989, we derived a single-cell subclone (A6-G3) in our laboratory[14]. We grew these cells at 37 °C in Tu2% medium (78% MCDB, 20% Leibovitz's L-15 medium, 2% FBS and 1.68 mM $CaCl_2$). We authenticated all cell lines via human short tandem repeat profiling. We periodically tested all cell lines for mycoplasma infections.

Plasmid construction and single guide RNA cloning. All the Cas9-positive melanoma cell lines in this study were derived by lentiviral transduction with a Cas9 expression vector (EFS-Cas9-P2A-Puro; Addgene, 108100). All the sgRNAs were cloned into a lentiviral expression vector (LRG2.1; Addgene, 108098), which contains an optimized sgRNA backbone. The annealed sgRNA oligonucleotides were ligated with T4 to the BsmB1-digested LRG2.1 vector. To improve U6 promoter transcription efficiency, an additional 5′ G nucleotide was added to all sgRNA oligonucleotide designs that did not already start with a 5′ G.

Construction of domain-focused single guide RNA pooled library. Gene lists of transcription factors, kinases and epigenetic regulators in the human genome were manually curated based on the presence of DNA-binding domain(s), kinase domains and epigenetic enzymatic/reader domains. The protein domain sequence information was retrieved from the NCBI Conserved Domains Database. Approximately six independent sgRNAs were designed against individual DNA-binding domains (Supplementary Tables 1–3)[27–29]. The design principle of sgRNA was based on previous reports, and the sgRNAs with the predicted high off-target effect were excluded[46]. For the initial pooled CRISPR screens, all of the sgRNAs oligonucleotides, including positive and negative control sgRNAs, were synthesized in a pooled format (Twist Bioscience) and then amplified by PCR. PCR-amplified products were cloned into a BsmB1-digested LRG2.1 vector using a Gibson Assembly kit (NEB, E2611). For the targeted pooled validation screens, individual sgRNAs were synthesized, cloned and verified via Sanger sequencing in a 96-well array platform (Supplementary Table 5). Individual sgRNAs were pooled in an equal molar ratio. To verify the identity and relative representation of sgRNAs in the pooled plasmids, a deep-sequencing analysis was performed on a MiSeq instrument (Illumina), confirming that 100% of the designed sgRNAs were cloned in the LRG2.1 vector and the abundance of >95% of individual sgRNA constructs was within fivefold of the mean (data not shown).

Lentivirus preparation. We produced lentivirus containing sgRNAs using HEK293T cells cultured in DMEM supplemented with 10% FBS and 1% penicillin–streptomycin. When the cells reached 90–100% confluency, we mixed the sgRNA vectors with the packaging vector psPAX2 and envelope vector pVSV-G in a 4:3:2 ratio in OPTI-MEM (Thermo Fisher Scientific, 31985070) and polyethylenimine (Polysciences, 23966). We collected viral supernatants for up to 72 h twice daily.

Transduction of spCas9. We introduced the stable expression of spCas9 via spinfection of lentivirus along with 5 μg ml^{-1} polybrene for 25 min at 1,750 r.p.m. We exchanged the medium ~6h after transduction and selected for cells expressing spCas9 via puromycin selection (1–2 μg ml^{-1}; 1 week). For WM989-A6-G3, we generated two cell lines, WM989-A6-G3-Cas9 and WM989-A6-G3-Cas9-5a3, the latter being a single-cell isolate of the bulk Cas9-expressing population. We verified that this cell line remained sensitive to PLX4032, that it still contained primed cells marked by the expression of drug-resistance markers and that it was capable of editing the genome (Extended Data Fig. 2). Following the same methodology, we generated a 451Lu-Cas9 cell line from 451Lu cells.

Transduction of lentivirus containing single guide RNAs. For transfection of melanoma cells, we infected cells with lentivirus and 5 μg ml^{-1} polybrene for 25 min at 1,750 r.p.m. We exchanged the medium ~6 h after transfection. We quantified the percentage of the population transfected by measuring the number of green fluorescent protein-positive cells at day 5 after transfection. For the screens, we aimed to transfect 30% of the population. For all other experiments, we aimed to transfect >95% of the population.

Initial pooled CRISPR screens. We worked with three main pooled sgRNA libraries in WM989-A6-G3-Cas9-5a3 cells. These libraries targeted ~2,000 different kinases, transcription factors and proteins involved in epigenetic regulation. In total, the libraries contained ~13,000 different sgRNAs, including nontargeting controls and controls that affect cell viability (Supplementary Tables 1–3). We aimed to transfect >1,000 cells for each sgRNA and isolated ~1,000 cells per sgRNA about a week after transfection and before any selection. These baselines allowed us to validate the efficiency of our screen by sgRNA enrichment/depletion of nontargeting controls and of controls that affect cell viability (Extended Data Fig. 2). Additionally, these baselines helped us to identify sgRNAs with lethal effects in our cells. Given that we were interested in rare-cell phenotypes that exist in a ratio of 1:2,000 cells or less, throughout our screens we expanded the population of cells to 50,000–250,000 cells per sgRNA, often surpassing a billion cells per screen. This scale allowed us to observe the rare-cell phenotypes dozens to hundreds of times in each of our controls (and in each sgRNA).

The priming screen aimed to identify perturbations that altered the frequency of $NGFR^{HIGH}/EGFR^{HIGH}$ cells. To this end, 1 month after we transfected and expanded the cells, we isolated the $NGFR^{HIGH}/EGFR^{HIGH}$ cells via magnetic-activated cell sorting followed by FACS (see below). We also collected an additional ~1,000 cells per sgRNA, without any selection, for comparison. Then, we isolated DNA from the cells and built sequencing libraries (see below) to quantify the representation of each sgRNA in the $NGFR^{HIGH}/EGFR^{HIGH}$ population and compare it to the unsorted baseline.

In the resistance screen, we aimed to identify proteins important for the development of resistance to vemurafenib. Here, we treated the cells as above, except that instead of isolating $NGFR^{HIGH}/EGFR^{HIGH}$ cells, we grew cells resistant to vemurafenib (see below) by exposing the cells to vemurafenib for 3 weeks. As above, we isolated DNA from the resulting population of cells and built sequencing libraries to quantify the representation of each sgRNA. The raw output of all screens was reads per sgRNA.

To select hits in our screens, we first normalized the output of our screens to reads per million and then calculated the fold change in sgRNA representation between different samples. For our priming screen, we focused on the fold change in sgRNA representation between $NGFR^{HIGH}/EGFR^{HIGH}$ cells and the bulk population of melanoma cells. For the resistance screen, we focused on the fold change in sgRNA representation between cells treated for 3 weeks with 1 μM vemurafenib and cells never exposed to the drug. After normalizing the change in sgRNA representation of each sgRNA by the median change across all sgRNAs, we organized our hits into tiers (1 through 4) based on the percentage of sgRNAs against the target exhibiting at least a twofold change in representation. We considered high-confidence hits those targets where (1) ≥75% (tier 1) or ≥66% (tier 2) of its sgRNAs showed at least a twofold enrichment/depletion throughout the screen and (2) no two sgRNAs showed a significant change (twofold change) in opposing directions (that is, one sgRNA is significantly enriched in the selected population while another one is significantly depleted). Other targets that showed a twofold enrichment/depletion throughout the screen, but in less than 66% of its sgRNAs, were considered lower confidence hits (tier 3 and tier 4). Note that we excluded from analysis any sgRNA with fewer than ten raw reads in all samples.

Secondary, targeted pooled CRISPR screen. To validate the replicability and generality of our hits, we designed a pool of sgRNAs for targeted screening that targeted proteins that either emerged as hits in our initial screens or did not pass our hit-selection criteria but changed the frequency of $NGFR^{HIGH}/EGFR^{HIGH}$ cells or the frequency of cells resistant to vemurafenib (Supplementary Table 5). In this pool, we included approximately three sgRNAs per protein target and carried out the screen in WM989-A6-G3-Cas9-5a3 cells, as well as in another $BRAF^{V600E}$ melanoma cell line, 451Lu-Cas9. As before, we conducted a priming screen where we isolated $NGFR^{HIGH}/EGFR^{HIGH}$ cells, as well as a resistance screen where we exposed cells to 1 μM vemurafenib for 3 weeks. Here too, we first normalized the output of our screens to reads per million and then calculated the fold change in sgRNA representation between different samples. Unlike on our initial screens, here we normalized the change in sgRNA representation to the median change in representation of the ten nontargeting sgRNA controls included in the screen.

Tumor growth assays in xenografts. All animal experiments were approved by the Institutional Animal Care and Use Committee (no. 112503X_0) and were performed in a facility accredited by the Association for the Assessment and Accreditation of Laboratory Animal Care. WM989-A6-G3-Cas9-5a3 human melanoma cells (1×10^6 cells) suspended in 100 μl of PBS were subcutaneously injected into 8-week-old NOD/SCID mice (Charles River Laboratories). When resulting tumors reached 150 mm^3, mice were fed either AIN-76A chow (untreated group, placebo) or AIN-76A chow containing 417 mg kg^{-1} PLX4720 (treated group). Tumor sizes were measured every 3–4 d using digital calipers, and tumor volumes were calculated using the following formula: volume = $0.5 \times (\text{length} \times \text{width}^2)$. Mice were euthanized when tumors reached ~1,500 mm^3 or upon development of skin necrosis. Throughout this time, the animal facility holding rooms were maintained between 70–73 °F and a humidity of 30–35%. The animal holding room light schedules were maintained on a 12-h on/off cycle with lights on from 6:00 to 18:00.

To assess growth differences between knockout and control tumors, for each mouse, we first quantified the change in tumor size from the initial time point to the time point in question as a $\log_2$ fold change in tumor volume. We determined the statistical significance of the differences observed between knockout and control at each therapy time point with a one-tailed *t*-test. For each knockout cell line, we then calculated the mean tumor volume and standard error of the

mean (Fig. 3). Note that within a given knockout-to-control comparison in each of the treatment arms, we defined the endpoint as the last point in time at which the number of mice in each group (knockout and control cell line) was at least three. The *n* at each time point and the respective *P* value are presented in Supplementary Table 7.

Immunostaining. For NGFR staining of fixed cells, after fixation and permeabilization, we washed the cells for 10 min with 0.1% BSA/PBS, and then stained the cells for 10 min with 1:500 anti-NGFR APC-labeled clone ME20.4 (BioLegend, 345107). After two final washes with PBS, we kept the cells in PBS. For EGFR and NGFR staining of live cells, we incubated melanoma cells in suspension for 1 h at 4 °C with 1:200 mouse anti-EGFR antibody, clone 225 (Millipore, MABF120) in 0.1% BSA/PBS. We then washed twice with 0.1% BSA/PBS and then incubated for 30 min at 4 °C with 1:500 donkey anti-mouse IgG-Alexa Cy3 (Jackson Laboratories, 715-545-150). We washed the cells again (twice) with 0.1% BSA/PBS and incubated for 10 min with 1:500 anti-NGFR APC-labeled clone ME20.4 (BioLegend, 345107). We again washed the cells twice with 0.1% BSA/PBS and finally resuspended them in 1% BSA/PBS.

Isolation of NGFR^{HIGH}/EGFR^{HIGH} cells. To enrich for NGFR^{HIGH}/EGFR^{HIGH} cells, we first immunostained melanoma cells as detailed above. Then, we used a manual separator for magnetic cell isolation (magnetic-activated cell sorting with LS columns and anti-APC microbeads from Miltenyi Biotec). In short, following the manufacturer's instructions, we incubated cells and microbeads at 4 °C for 15 min, then washed and pelleted the cells via centrifugation. After resuspending the cells, we passed them through LS magnetic columns. After enriching for NGFR^{HIGH} cells, we proceeded to select only the cells expressing both NGFR and EGFR via FACS (MoFlo Astrios EQ).

Growth of resistant colonies. To grow melanoma cells resistant to BRAF^{V600E} inhibition, we exposed melanoma cells to 1 μM vemurafenib (PLX4032; Selleckchem, S1267) for 2–3 weeks. For the combined BRAF^{V600E} and MEK inhibition assays, we also used dabrafenib at 500 nM and 100 nM (GSK2118436; Selleckchem, S2807), trametinib at 5 nM and 1 nM (GSK1120212; Selleckchem, S2673) and cobimetinib at 10 nM and 1 nM (GDC-0973, Selleckchem, S8041).

Inhibition of DOT1L via small-molecule inhibitor. For all assays involving pharmacological inhibition of DOT1L, we used pinometostat at concentrations ranging from 1 μM to 5 μM (EPZ5676; Selleckchem, S7062).

MiSeq library construction and sequencing. To quantify the sgRNA representation following selection in our screen, we sequenced the sgRNAs according to work by Shi et al.[47]. In short, we isolated genomic DNA using the Quick-DNA Midiprep Plus Kit (Zymo Research, D4075) per the manufacturer's specifications. We then performed PCR amplification of the sgRNAs using Phusion Flash High Fidelity Master Mix Polymerase (Thermo Scientific, F-548L) and primers that incorporate a barcode and a sequencing adaptor to the amplicon. Our amplification strategy consisted of an initial round of parallel PCRs (23–29 cycles of up to 200 parallel reactions per sample. We then pooled the PCR reactions and purified them using the NucleoSpin Gel and PCR clean-up kit (Macherey-Nagel, 740609.250). We continued with eight PCR cycles using Phusion Flash High Fidelity Master Mix Polymerase, followed by column purification with the QIAquick PCR Purification Kit (QIAGEN, 28106). We quantified the sgRNA libraries with the DNA 1000 Kit (Agilent, 5067-1504) on a 2100 Bioanalyzer Instrument (Agilent, G2939BA). We pooled the barcoded sgRNA libraries and sequenced via 150-cycle paired-end sequencing (MiSeq Reagent Kit v3; Illumina, MS-102-3001). We then mapped the resulting sequences to our reference sgRNA library and proceeded to select hits.

Cell fixation and permeabilization. For the imaging assays, we fixed cells for 10 min with 4% formaldehyde and permeabilized them with 70% ethanol overnight.

Colony formation assays. For each condition tested, we first split cells into two to four six-well plates at ~10,000–50,000 cells per well. We fixed and permeabilized one of the replicates to use as a baseline (number of cells plated before testing) and exposed the rest to the test condition. At the endpoint, we fixed and permeabilized the rest of the samples.

Image analysis of NGFR immunostains. We developed a custom MATLAB pipeline for counting cells and quantifying immunofluorescence signal of DAPI-stained and NGFR-stained cells (https://github.com/arjunrajlaboratory/). The software stitches together a large tiled image, then uses DAPI to identify cells. Using the nuclear area, it then looks at a set of pixels near the nucleus to quantify fluorescence intensity of the NGFR staining. After quantifying the expression level of NGFR following knockout of select screen targets and of nontargeting controls, we quantified the minimum expression level needed to be considered an NGFR^{HIGH} cell. First, we selected the top 1% highest expressors of NGFR in each of our nontargeting negative controls. Then, within that top 1%, we obtained the median expression level of the lowest expressor across all controls, and used that as a threshold to quantify the frequency of NGFR^{HIGH} cells in each of our knockout samples. Next, we calculated the change in frequency of NGFR^{HIGH} cells in each test condition compared to controls and obtained a median fold change and standard deviation across all samples with knockout of one same protein (~3 different biological samples per protein). In total, we targeted ~86 different proteins across ~258 different knockout biological samples.

Image analysis of colony formation. We developed a custom MATLAB pipeline for counting cells and colonies in tiled images of DAPI-stained cells (https://github.com/arjunrajlaboratory/). First, the software stitches the individual image tiles into one large image by automatically (or with user input) determining the amount of overlap between each individual image. Then, the software identifies the location of each cell in the stitched image by searching for local maxima. We then manually identified the colony boundaries and quantified the number of colonies in each sample. We then calculated the frequency of resistant colonies by dividing the number of colonies by the total number of cells present in the culture before BRAF^{V600E} inhibition. Finally, we scaled the frequency of colonies to colonies per 10,000 cells and calculated the change in frequency between each sample and the median change across controls.

RNA sequencing and identification of differential expression. We sequenced mRNA in bulk from WM989-A6-G3 and WM989-A6-G3-Cas9 populations according to work by Shaffer et al.[14]. In addition to quantifying the transcriptome of EGFR^{HIGH}, NGFR^{HIGH}, NGFR^{HIGH}/EGFR^{HIGH} and vemurafenib-resistant cells, we quantified the transcriptional changes following the knockout of many tier 1 and tier 2 hits from both the priming and resistance screens. In addition to hits from our screens, we also quantified the transcriptome of targets that were not tier 1 or tier 2 hits, but showed a change in the frequency of NGFR^{HIGH}/EGFR^{HIGH} cells or of cells resistant to vemurafenib. In total, we targeted ~83 different proteins, each in triplicate (using different sgRNAs) for a total of 280+ RNA-sequencing (RNA-seq) samples. For each sample, we isolated mRNA and built sequencing libraries using the NEBNext Poly(A) mRNA Magnetic Isolation Module and NEBNext Ultra RNA Library Prep Kit for Illumina per the manufacturer's instructions. We then sequenced the libraries via paired-end sequencing (36×2 cycles) on a NextSeq 500. We aligned reads to hg19 and quantified reads per gene using STAR and HTSeq. Finally, we used DEseq2 to identify differentially expressed genes.

Gene-set enrichment analysis. To identify 'biological signatures' enriched or depleted following the knockout of a given target, we used the GSEA software (http://software.broadinstitute.org/gsea/index.jsp). We focused on the biological process ontology of the GO gene sets (c5.bp.v6.2.symbols from https://www.gsea-msigdb.org/gsea/msigdb/collections.jsp#C5/) to obtain enrichment scores.

Grouping of targets based on transcriptomic analysis. To group targets into classes based on their transcriptional effects, we clustered all RNA-seq samples (hierarchical clustering via pheatmap in R) based on the change in expression (as obtained by DEseq2) of any gene differentially expressed (twofold change versus control, with an adjusted $P \leq 0.05$) in at least one of the 83+ knockouts. We also grouped targets via pheatmap based on the enrichment scores obtained via GSEA. To identify the axes that accounted for the variability between each knockout, we also performed principal-component analysis based on the gene-set enrichment scores of each knockout. Note that in the aforementioned analysis we included the transcriptomes of primed cells (marked by the expression of EGFR alone, NGFR alone, and NGFR and EGFR in combination) and of cells resistant to vemurafenib.

Reporting Summary. Further information on research design is available in the Nature Research Reporting Summary linked to this article.

Data availability

All data used in this work can be found at https://www.dropbox.com/sh/t08558cl4mepfm6/AABBvbtlTPSNNPoMC9NTro-9a?dl=0/. RNA-seq data are also deposited at the Gene Expression Omnibus (GSE151825 and GSE149280). The gene sets used for analysis were obtained from https://www.gsea-msigdb.org/gsea/msigdb/collections.jsp#C5/.

Code availability

All custom code used in this work is available at https://github.com/edatorre/2020_TorreEtAl_data.git/ and https://www.dropbox.com/sh/t08558cl4mepfm6/AABBvbtlTPSNNPoMC9NTro-9a?dl=0/. The software used for image analysis can be found at https://github.com/arjunrajlaboratory.

References

46. Hsu, P. D. et al. DNA targeting specificity of RNA-guided Cas9 nucleases. *Nat. Biotechnol.* **31**, 827–832 (2013).
47. Shi, J. et al. Discovery of cancer drug targets by CRISPR–Cas9 screening of protein domains. *Nat. Biotechnol.* **33**, 661–667 (2015).

Acknowledgements

We thank M. Herlyn for always providing excellent advice and guidance. We also thank the Flow Cytometry core team, especially F. Tuluc, at the Children's Hospital of Philadelphia for all their advice and help. We also thank all members of the Raj laboratory, as well as J. Murray, for their comments and suggestions. We thank C. Vakoc for providing the transcription factor, epigenetic regulator and kinase domain-focused sgRNA library. C.L.J. acknowledges the National Institutes of Health (NIH) awards T32 DK007780 and F30 HG010822. B.L.E. acknowledges support from NIH training grants F30 CA236129, T32 GM007170 and T32 HG000046. S.M.S. acknowledges support from DP5 OD028144. I.A.M. acknowledges funding from the NIH and the National Institute of Neurological Disorders (F30NS100595). A.T.W. and M.E.F. are supported by R01CA207935. A.T.W. and G.M.A. are supported by P01 CA114046, and A.T.W. is supported by CA227550, CA232256, the E.V. McCollum Chair and a Bloomberg Distinguished Professorship. Core facilities used in this grant are supported by P30CA010815 and P30CA006973. J.S. acknowledges support from the Linda Pechenik Montague Investigator Award and Cold Spring Harbor Laboratory sponsored research. A.R. acknowledges R01 CA238237, a NIH/National Cancer Institute Physical Science–Oncology Centers award (U54 CA193417), a National Science Foundation CAREER award (1350601), P30 CA016520, SPORE P50 CA174523, NIH U01 CA227550, NIH 4DN U01 HL129998, NIH Center for Photogenomics (RM1 HG007743) and the Tara Miller Foundation.

Author contributions

E.A.T., J.S. and A.R. designed and supervised the study. E.A.T. performed the experiments and analysis. E.A. and K.A.B. assisted with CRISPR screens. S.B. and C.L.J. assisted with tissue culture, image acquisition and analysis. L.E.B. designed image analysis software. M.E.F. and G.M.A. performed in vivo assays. B.L.E. and S.M.S. assisted with acquisition of transcriptomic data. B.L.E., S.M.S. and I.A.M. assisted with data analysis. A.T.W. provided guidance on interpretation of the data.

Competing interests

A.R. and S.M.S. receive patent royalty income from LGC/Biosearch Technologies related to Stellaris RNA FISH probes. All other authors declare no competing interests.

Additional information

Extended data is available for this paper at https://doi.org/10.1038/s41588-020-00749-z.

Supplementary information is available for this paper at https://doi.org/10.1038/s41588-020-00749-z.

Correspondence and requests for materials should be addressed to J.S. or A.R.

Reprints and permissions information is available at www.nature.com/reprints.

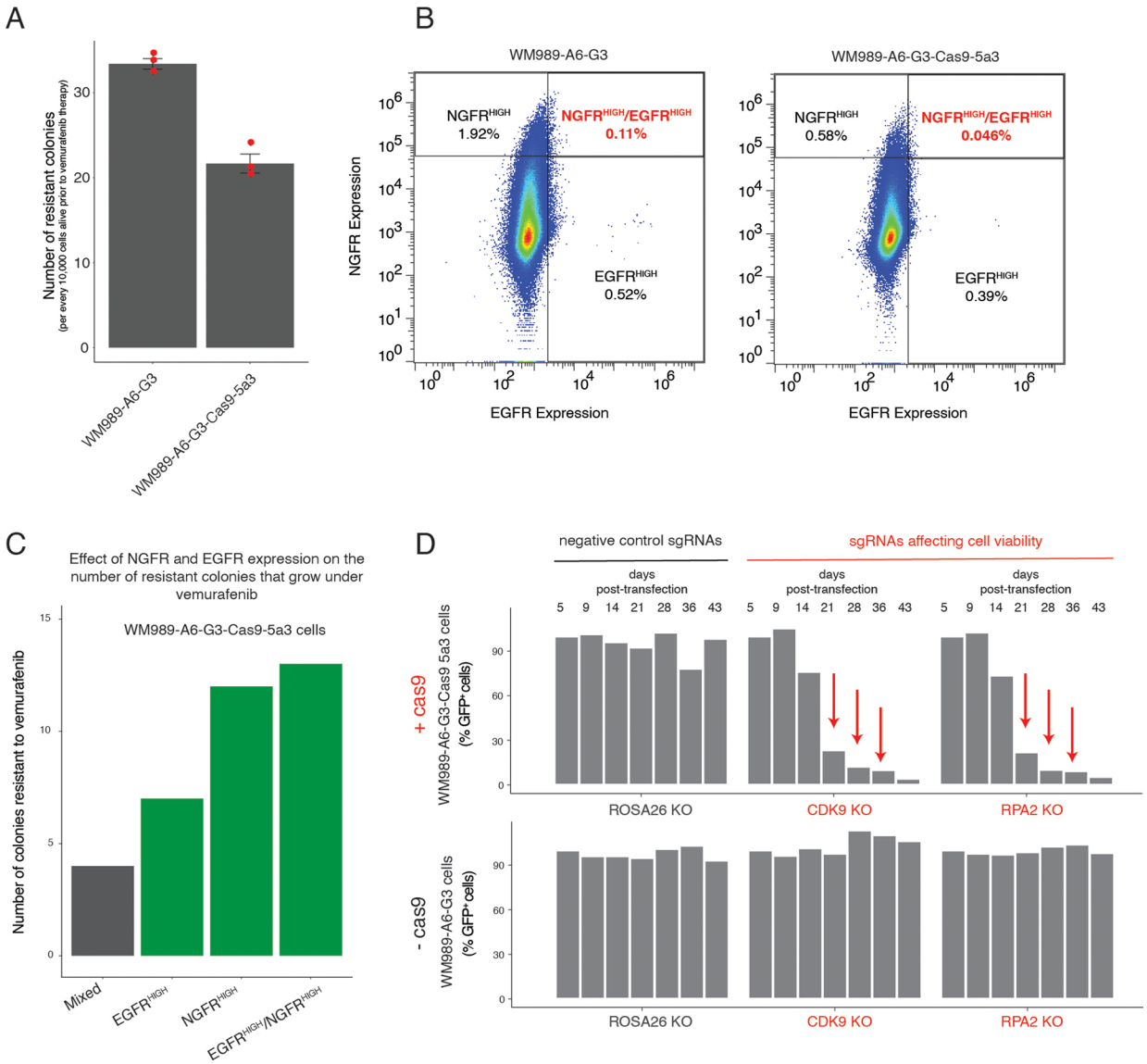

Extended Data Fig. 1 | Technical validation of WM989-A6-G3-Cas9-5a3 cell line. a, To compare the frequency of drug resistance between WM989-A6-G3 and its daughter cell line WM989-A6-G3-Cas9-5a3, we cultured an equal number of cells from each cell line in 1 μM vemurafenib for 3 weeks. Then, we counted the number of colonies that resulted from each cell line. Each dot represents the number of resistant colonies normalized to 10,000 cells alive in each sample before the addition of vemurafenib. The bars represent the mean number of colonies over triplicates, normalized to 10,000 cells alive in each sample before the addition of vemurafenib. Error bars represent the standard error of the mean. **b**, To compare the frequency of NGFR^{HIGH}/EGFR^{HIGH} cells between WM989-A6-G3 and its daughter cell line WM989-A6-G3-Cas9-5a3, we looked at the distribution of expression of NGFR and EGFR using immunofluorescence. **c**, WM989-A6-G3-Cas9-5a3 cells expressing NGFR, EGFR, and both NGFR and EGFR are more likely to survive and proliferate in the presence of vemurafenib[14]. Here, we show the number of colonies that grew upon vemurafenib exposure in a mixed population of WM989-A6-G3-Cas9-5a3 or in the same population but enriched for EGFR^{HIGH} cells, NGFR^{HIGH} cells, or NGFR^{HIGH}/EGFR^{HIGH} cells. **d**, In this plot, we show the single guide RNA representation (as percent GFP-positive cells) of controls over time in WM989-A6-G3 cells with or without Cas9 expression. Negative controls (black) are single guide RNAs aimed at *ROSA26*, a non-expressing gene in human melanoma. Positive controls (red) target proteins necessary for cell viability. Only cells expressing both Cas9 and a positive control single guide RNA should disappear from the population over time.

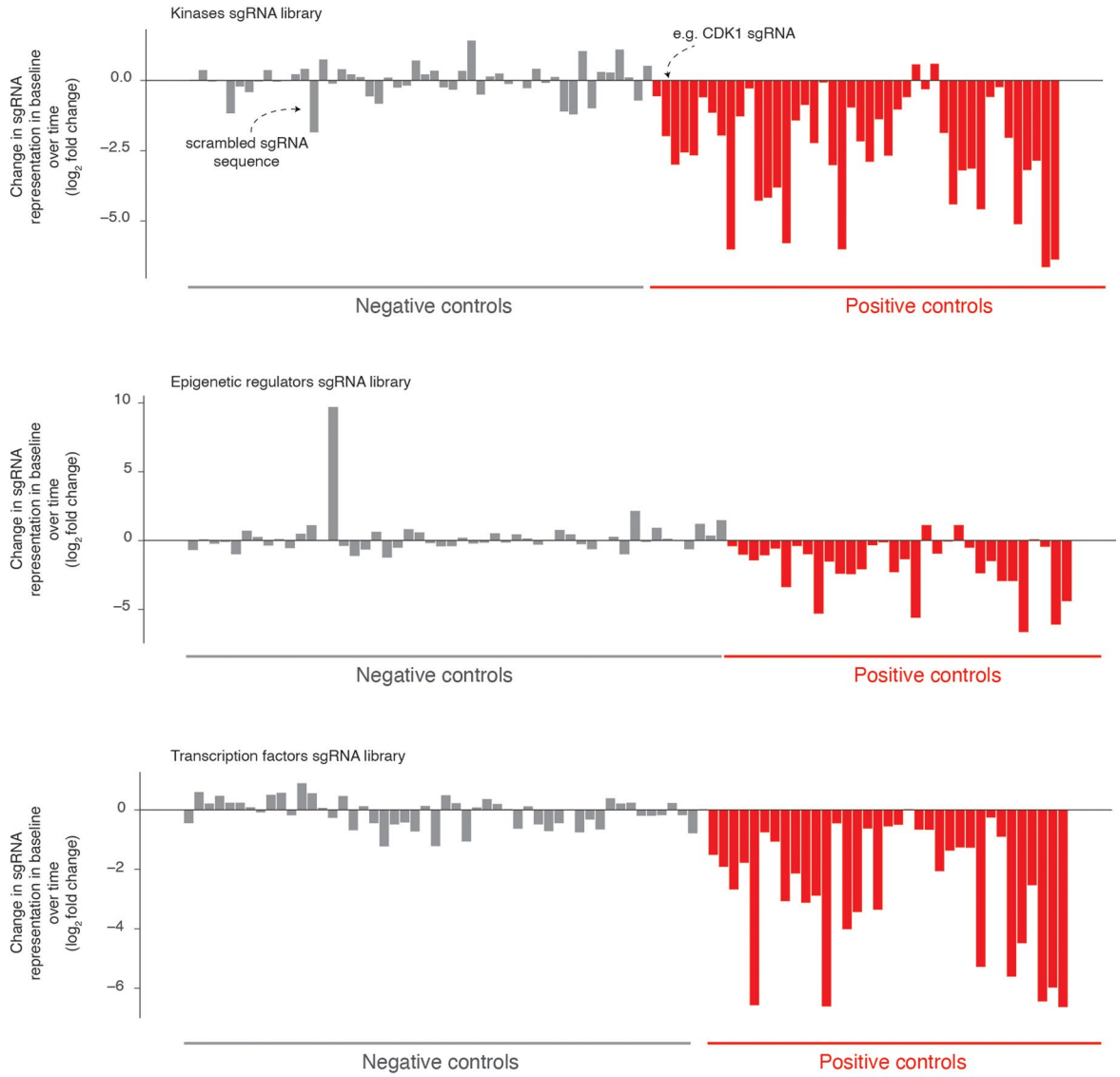

Extended Data Fig. 2 | Effect of negative and positive control single RNAs in the CRISPR screens. Our pooled CRISPR screen included non-targeting single guide RNAs as negative controls (gray bars, 50+ single guide RNAs) as well as single guide RNAs affecting cell viability as positive controls (red bars, 25+ single guide RNAs). We quantified the change in representation of these single guide RNAs over time and report the $\log_2$ fold change in representation from 6 days after transfection to right before selection (vemurafenib exposure or selection by NGFR and EGFR expression). We expect positive controls to lose representation over time more often than negative controls. Our screening scheme utilized three separate pooled single guide RNA libraries, one targeting kinases (top), another targeting epigenetic domains (middle), and a final one targeting transcription factors (bottom).

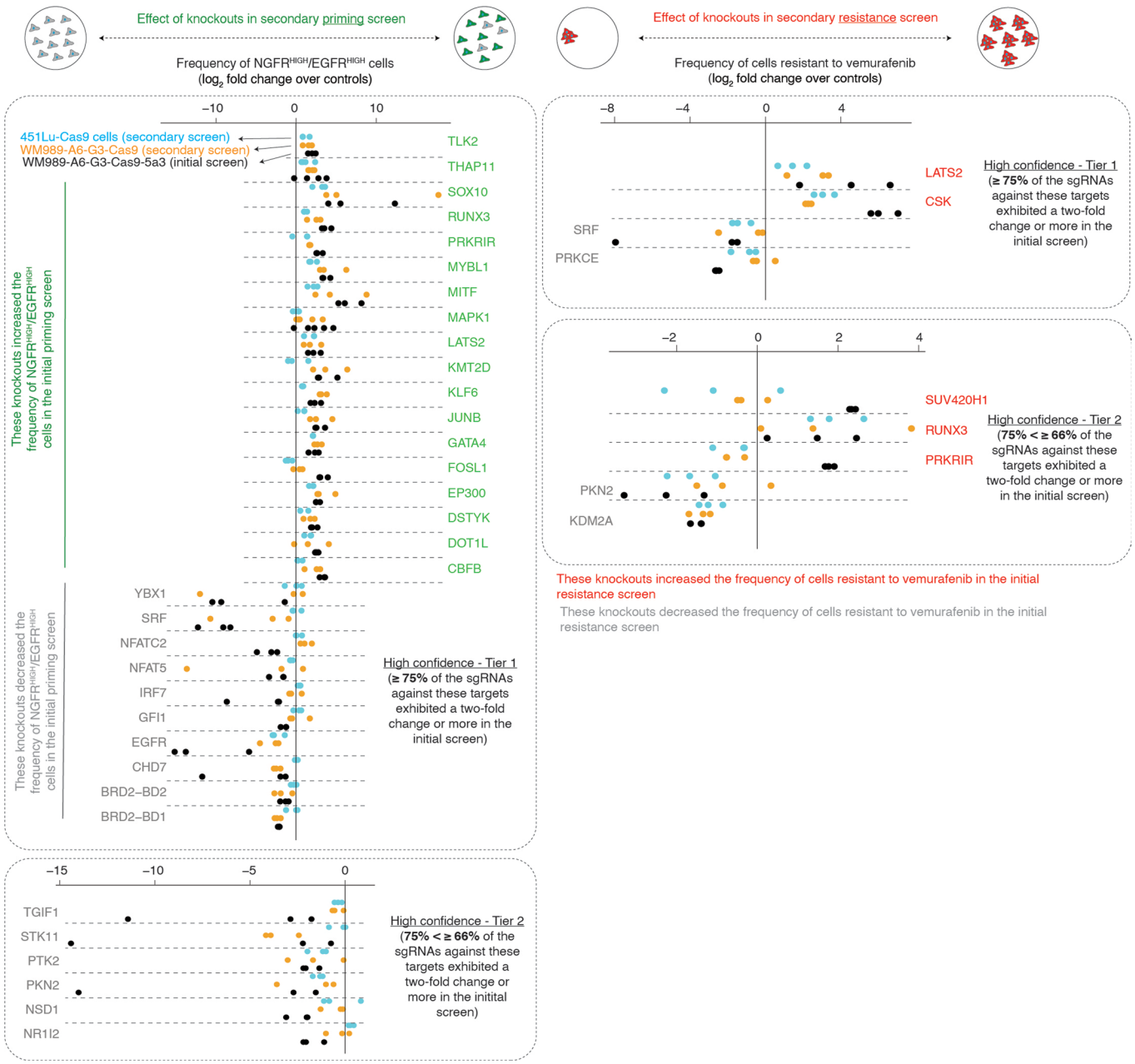

Extended Data Fig. 3 | Secondary validation of hits across multiple cell lines by secondary targeted CRISPR screening. We assessed the robustness and generality of the effect of hits identified in the priming and resistance screens (WM989-A6-G3-Cas9-5a3, black bars) by carrying out secondary priming (left) and resistance screens (right) targeting 86 different proteins in WM989-A6-G3-Cas9 (orange bars) as well as in another BRAF^{V600E} melanoma cell line (451Lu-Cas9, blue). On the left, we plot the $\log_2$ fold change in frequency of NGFR^{HIGH}/EGFR^{HIGH} cells (normalized by non-targeting controls) for each sgRNA (dots) targeting 34 of the high confidence hits (Tiers 1 and 2) we identified in the priming screen. We found that 25 of the 34 high confidence hits showed at least a two fold change (as a median across sgRNA triplicates; see Supplementary Table 4) in the frequency of NGFR^{HIGH}/EGFR^{HIGH} cells concordant with the effects detected in the original screening clonal cell line (WM989-A6-G3-Cas9-5a3). In 451Lu-Cas9 cells, 20 of the 34 targets also showed a change in the frequency of NGFR^{HIGH}/EGFR^{HIGH} cells, with 11 of those exhibiting at least a two-fold change (as a median across sgRNA triplicates; see Supplementary Table 4). On the right, we plot the $\log_2$ fold change in frequency of cells resistant to vemurafenib (normalized by non-targeting controls) for each sgRNA (dots) targeting 9 of the high confidence hits (Tiers 1 and 2) identified through the resistance screen. In WM989-A6-G3-Cas9, we found that 7 of the 9 targets replicated the effect we observed originally. For 451Lu-Cas9, the same 7 factors showed similar effects. Within each plot, the color of the target label indicates the effect observed in the primary screens. See Supplementary Table 4 for the results of Tier 3 and Tier 4 targets.

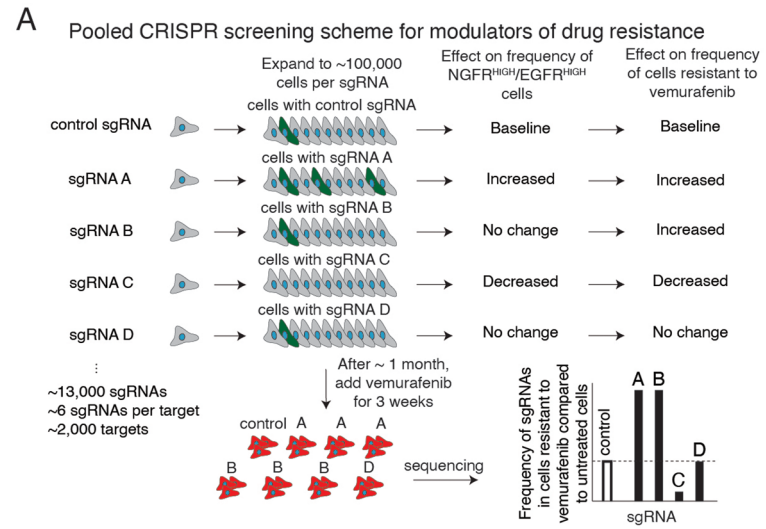

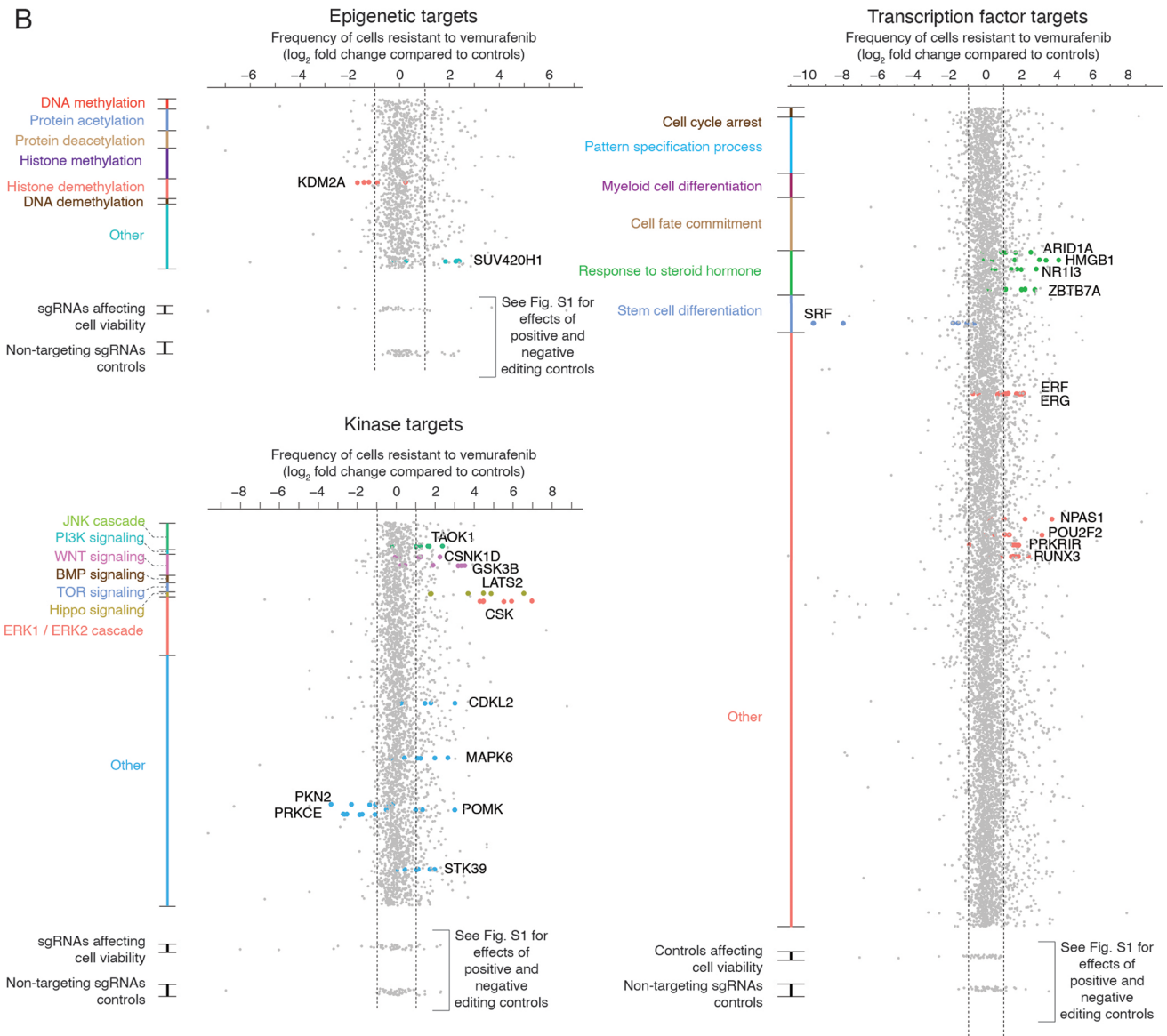

Extended Data Fig. 4 | See next page for caption.

Extended Data Fig. 4 | Screen for factors modulating number of resistant colonies upon BRAF^{V600E} inhibition. a, We performed a pooled CRISPR screen to detect modulators of the number of drug-resistant cells that grow in the presence of the BRAF^{V600E} inhibitor vemurafenib. After transducing a library of single guide RNAs and expanding the population, we exposed the cells to the BRAF^{V600E} inhibitor vemurafenib (1 μM) for 3 weeks, after which we sequenced the single guide RNAs in the surviving population. Changes in the frequency of detection of a given single guide RNA indicates that its target may affect the ability of a cell to survive and proliferate upon BRAF^{V600E} inhibition. **b**, After transfecting a population of melanoma cells, we exposed them to vemurafenib (BRAF^{V600E} inhibitor, 1 μM) for 3 weeks to grow resistant colonies. We then sequenced the DNA to quantify the single guide RNA representation of each target in the resulting population, using the same libraries as in Fig. 1. As before, we ranked the targets into tiers based on the percent of single guide RNAs that exhibited at least a two-fold change in representation throughout the screen (Tier 1, ≥ 75%; Tier 2, ≥ 66%; Tier 3, ≥ 50%; Tier 4, < 50%), thus reflecting the degree of confidence we have in the hit (High confidence hits: Tiers 1 and 2; Low confidence hits: Tiers 3 and 4). In this screen, we identified 24 high confidence factors. For a more detailed description, see the Methods section.

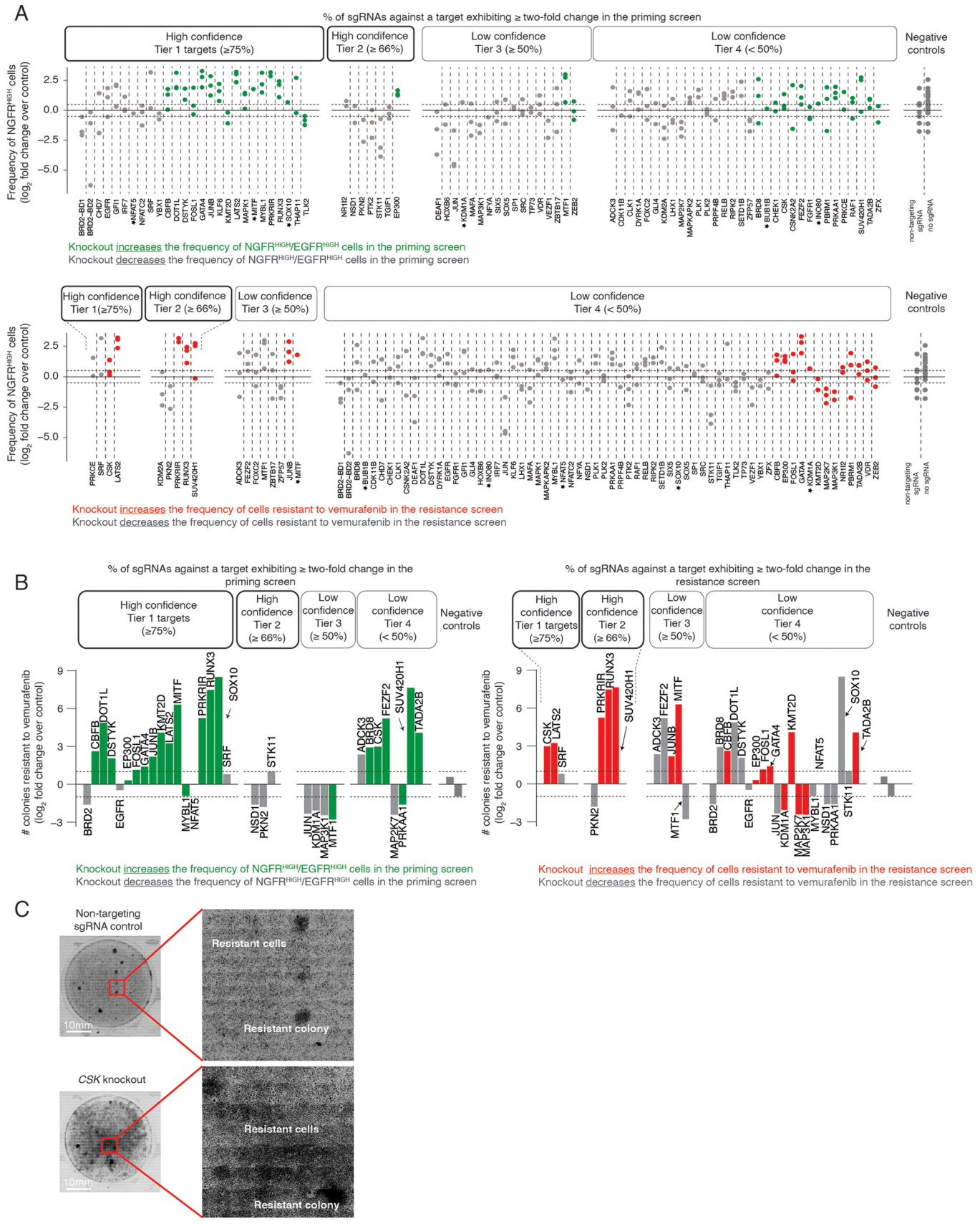

Extended Data Fig. 5 | See next page for caption.

Extended Data Fig. 5 | Validation of effects of hits from priming and resistance screens by via NGFR immunofluorescence and resistant colony formation. a, Frequency of NGFR^{HIGH} cells following the knockout of select targets. Dots represent the change in number of NGFR^{HIGH} cells (as the $\log_2$ fold change over non-targeting sgRNA controls). A star indicates targets where, after excluding samples with low cell numbers (< 500 cells), $n=1$. Tier refers to the degree of confidence we have in each particular hit (see Methods). We performed this analysis for hits from both the priming screen (top) and the resistance screen (bottom). 21 of 34 high confidence showed at least a 50% increase or decrease in the frequency of NGFR^{HIGH} cells (see Supplementary Table 4). 21 of 49 targets from Tiers 3 and 4 increased or decreased the frequency of NGFR^{HIGH} cells by ≥ 50%. **b**, Resistance phenotype of melanoma cells following the knockout of hits. Bars represent the $\log_2$ fold change over non-targeting control in the number colonies able to grow in vemurafenib. The number of colonies is normalized to the number of cells present before BRAF^{V600E} inhibition (see Methods). In the left panel, we labeled in green and gray the effect a given target has on the frequency of NGFR^{HIGH}/EGFR^{HIGH} cells (based on the initial priming screen). In the right panel, we labeled in red and gray the effect a given target has on the number of cells that resist BRAF^{V600E} inhibition (based on the initial resistance screen). Each bar represents one experimental replicate (see Extended Data Fig. 6b for replicates). **c**, These images show the effect of CSK knockout on a cell's ability to develop resistance to BRAF^{V600E} inhibition. We exposed CSK-knockout WM989-A6-G3-Cas9-5a3 cells to 1 μM vemurafenib for 3 weeks and counted the number of resulting colonies. The number of resistant cells is too large to accurately identify individual colonies; thus, the number of colonies reported is an underestimate.

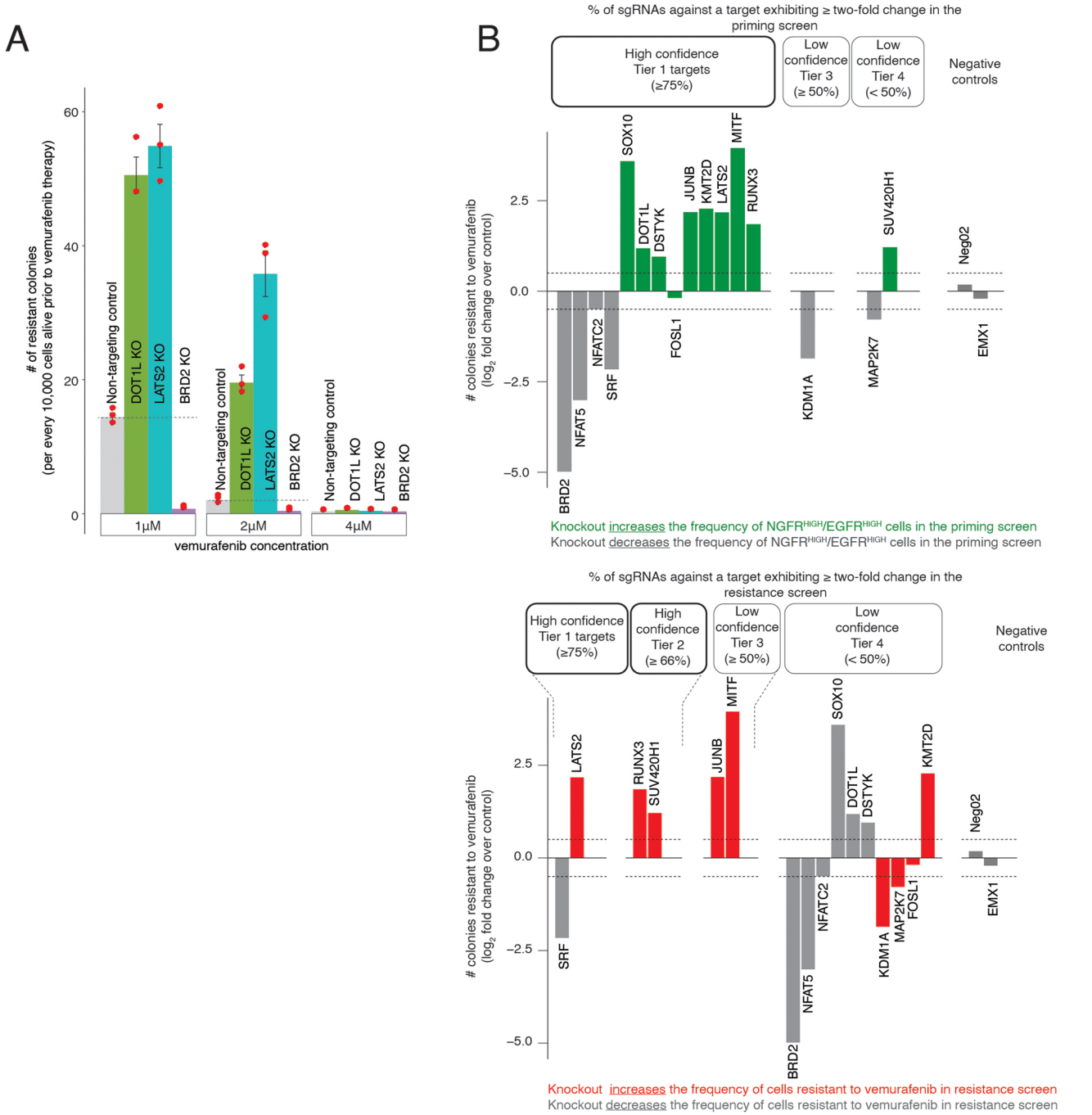

Extended Data Fig. 6 | Validation of effects of hits by resistant colony formation. a, Effect of vemurafenib concentration on the formation of drug-resistant colonies. The dots represent the number of resistant colonies that grow after 3 weeks of treatment with 1 μM, 2 μM, or 4 μM of PLX4032 (vemurafenib). The bars represent the mean over three biological replicates. Error bars represent the standard error. At each concentration, we treated cells that contain either a non-targeting sgRNA, or a sgRNA targeting *DOT1L*, *LATS2*, or *BRD2*. **b**, Resistance phenotype of melanoma cells following the knockout of hits from the initial screens. Each bar represents the $\log_2$ fold change over non-targeting control in the number of colonies able to grow following knockout of the gene indicated. The number of colonies for each target is normalized to the number of cells present in culture before $BRAF^{V600E}$ inhibition, reported as number of colonies per every 10,000 pre-treatment cells (see Methods). As before, the different tiers represent the percent of single guide RNAs against a given target exhibiting at least a two-fold change throughout the initial (top) priming or (bottom) resistance screens. In the top panel, we labeled in green and gray the effect a given target has in the frequency of $NGFR^{HIGH}/EGFR^{HIGH}$ cells (based on the initial priming screen). In the bottom panel, we labeled in red and gray the effect a given target has in the number of cells that resist $BRAF^{V600E}$ inhibition (based on the resistance screen). In this plot, each bar represents one experimental replicate (distinct from the one in Extended Data Fig. 5b).

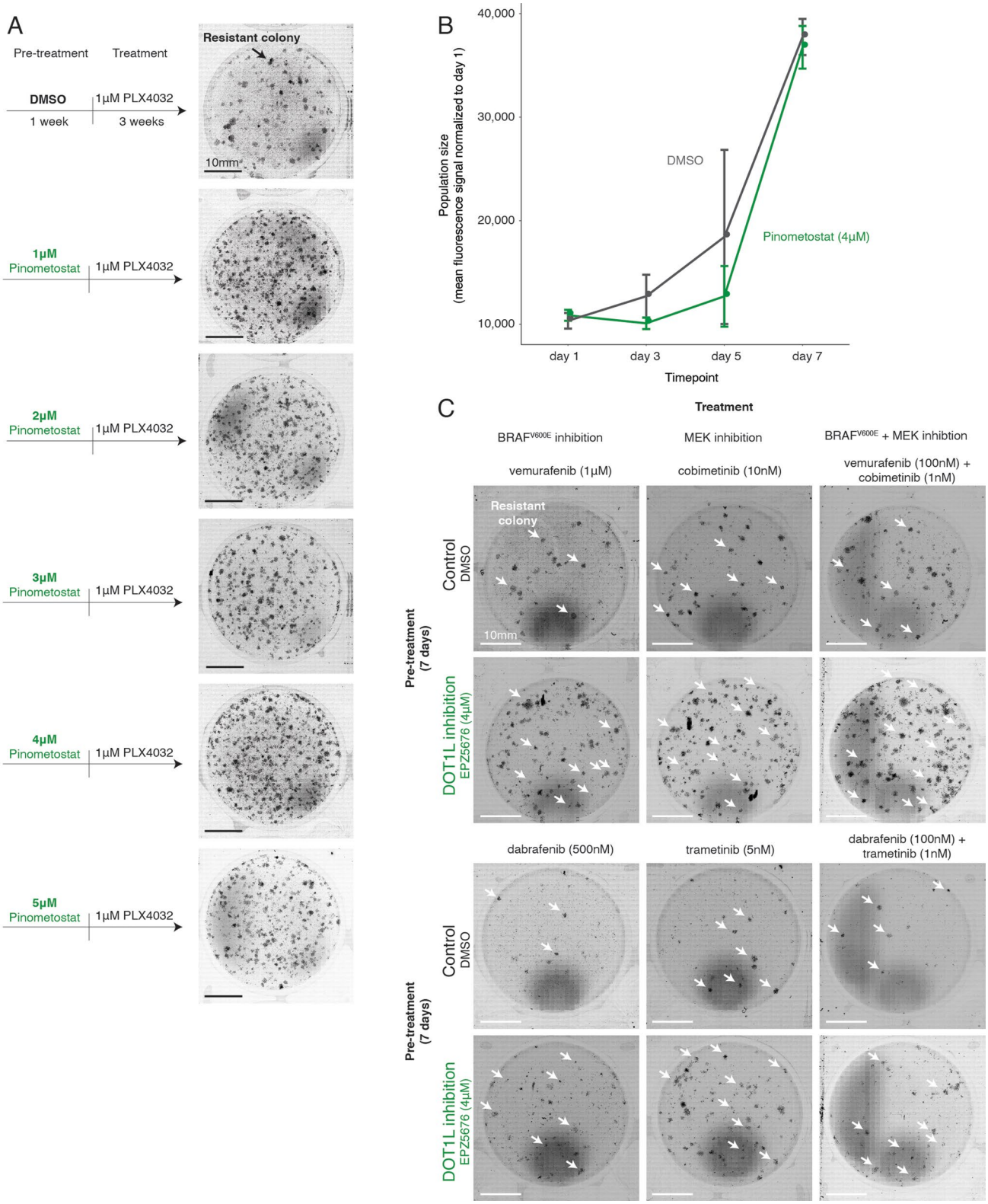

Extended Data Fig. 7 | See next page for caption.

Extended Data Fig. 7 | Effect of pharmacological inhibition of DOT1L on resistance to BRAF^{V600E} and MEK inhibition. a, Resistance phenotype of melanoma cells following pharmacological inhibition of DOT1L. We pre-treated melanoma cells for seven days with either DMSO, or various concentrations of the DOT1L inhibitor pinometostat (EPZ5676). Then, we exposed the cells to 1 μM vemurafenib for 3 weeks. **b**, To assess the effect of DOT1L inhibition on cellular proliferation, we compared the population size of WM989-A6-G3 cells over time treated with either 4 μM of pinometostat (DOT1L inhibitor) or DMSO. The population size is estimated by the amount of nucleic acids present in the population using a CyQuant GR dye. The values represent mean fluorescent signal over triplicates. Error bars represent standard error of the mean. **c**, Resistance phenotype of melanoma cells to BRAF^{V600E} and MEK inhibitors following pharmacological inhibition of DOT1L. We pre-treated melanoma cells for seven days with either DMSO or 4 μM of pinometostat. We then exposed the cells to one of two BRAF^{V600E} inhibitors (vemurafenib and dabrafenib, left panels), to one of two MEK inhibitors (cobimetinib and trametinib, middle panels), or to a combination of a BRAF^{V600E} and MEK inhibitor (vemurafenib + cobimetinib; dabrafenib + trametinib, right panels). White arrows point to a few of the many colonies that grew under each condition.

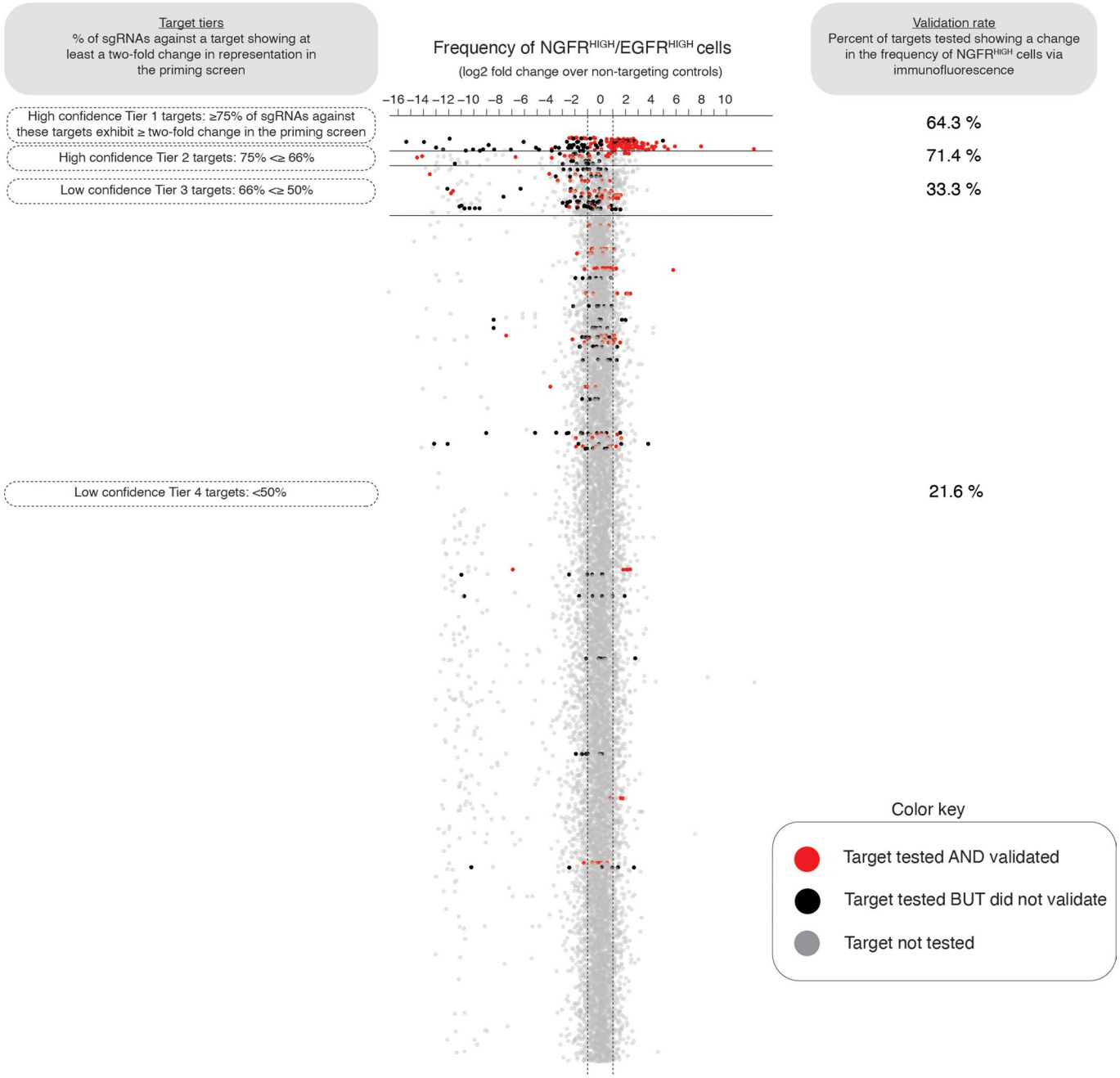

Extended Data Fig. 8 | Percent of targets from the priming screen that validate. To assess the sensitivity of our screen, we validated the effect observed in the initial priming screen for a select group of targets via NGFR immunofluorescence. Here, each dot represents an individual single guide RNA, and we plot the change in single guide RNA representation between NGFR^{HIGH}/EGFR^{HIGH} cells and controls (as measured in the priming screen). We then organize all sgRNAs into tiers (*y*-axis, Tiers 1 through 4) based on the percent of single guide RNAs against a target showing at least a two-fold change in representation on NGFR^{HIGH}/EGFR^{HIGH} cells. In red, we labeled targets that when tested again produced at least a 50% change in the frequency of NGFR^{HIGH} cells. In black, we labeled targets that we tested but did not validate, and in gray we show targets we did not test. We display the percent of genes tested and validated at each tier on the right.

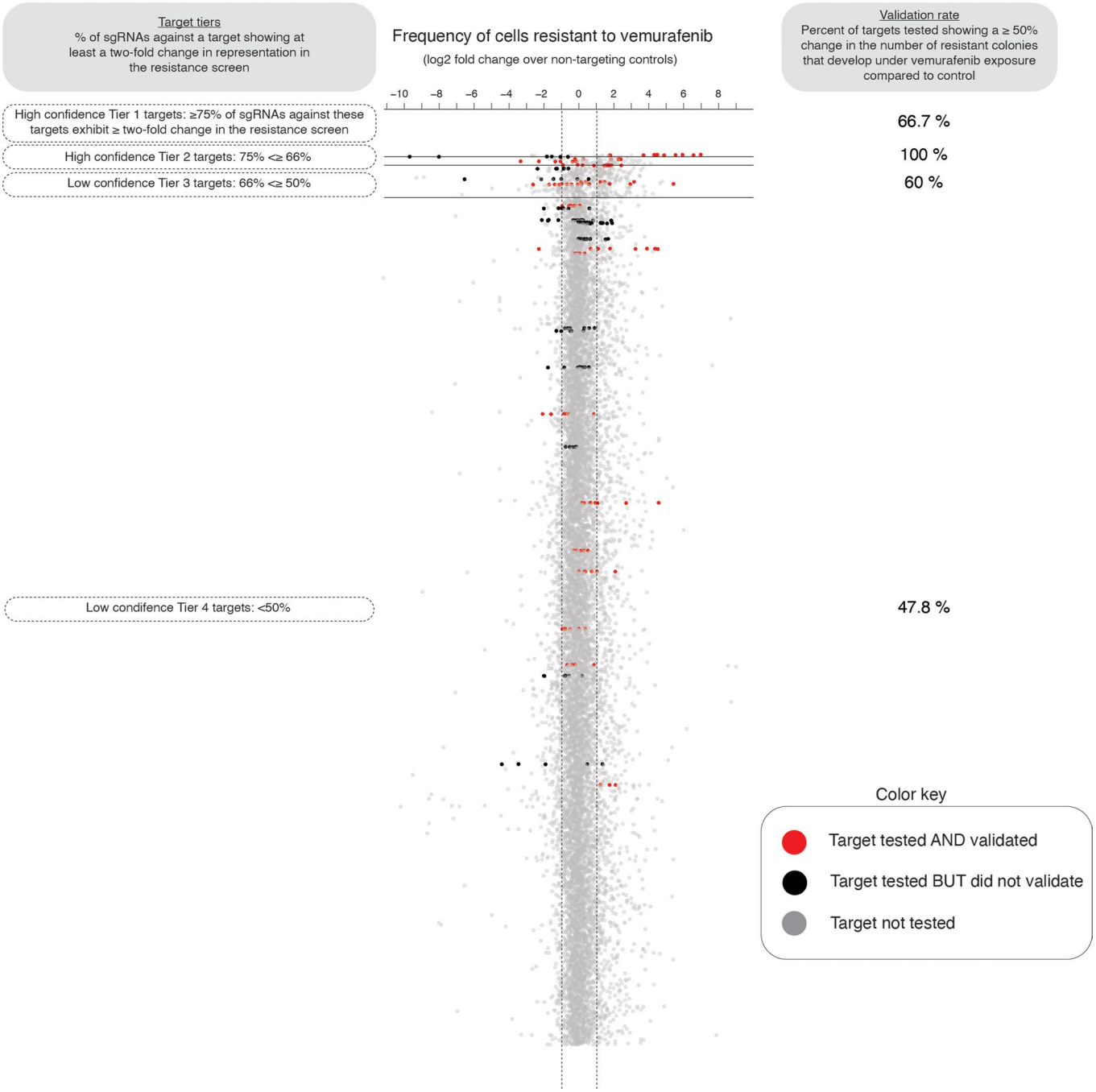

Extended Data Fig. 9 | Percent of targets from the resistance screen that validate. To assess the sensitivity of our screen, we validated the effect observed in the initial resistance screen for a select group of targets via colony formation assays. Here, each dot represents an individual single guide RNA, and we plot the change in single guide RNA representation between cells resistant to vemurafenib and cells that have never been exposed to the drug (as measured in the resistance screen). We then organize all single guide RNAs into tiers (*y*-axis, Tiers 1 through 4) based on the percent of single guide RNAs against a target showing at least a two-fold change in representation on drug resistant cells. In red, we labeled targets that when tested again produced at least a 50% change in the frequency colonies resistant to $BRAF^{V600E}$ inhibition. In black, we labeled targets that we tested but did not validate, and in gray we show targets we did not test. We display the percent of genes tested and validated at each tier on the right.

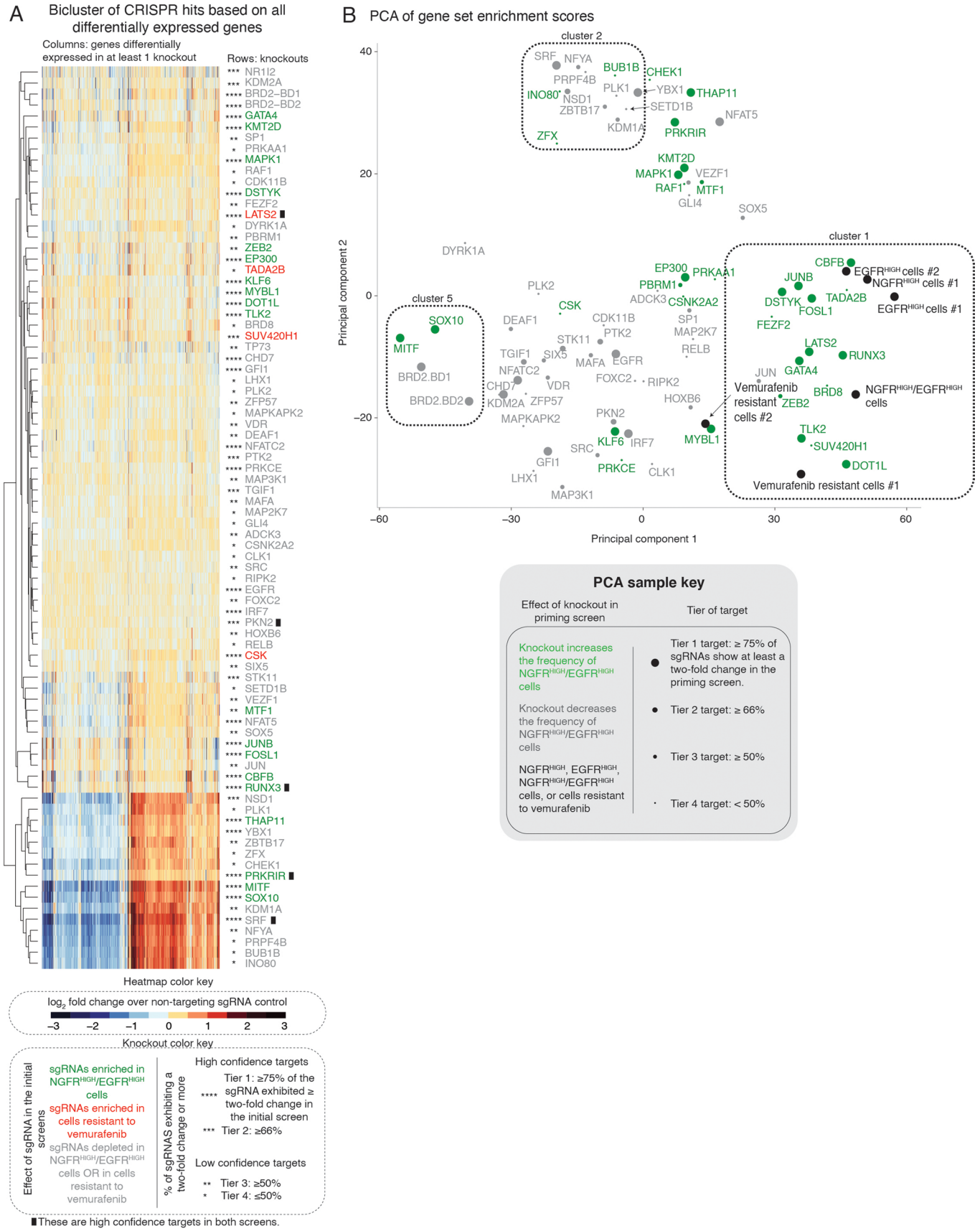

Extended Data Fig. 10 | See next page for caption.

Extended Data Fig. 10 | Transcriptional effects induced by knockout of select screen targets. a, The heatmap represents the biclustering analysis of different screen targets (rows) based on the change in expression of all genes differentially expressed in at least one knockout (columns). Within the heatmap, red indicates an increase in expression following the knockout, while blue indicates a decrease in gene expression (see heatmap color key). Each target (rows) represents transcriptomes of biological triplicates (unless otherwise stated in Supplementary Table 4). Target labels (rows) in green indicate genes whose knockout increased the frequency of $NGFR^{HIGH}/EGFR^{HIGH}$ cells in the initial screen. In red are those whose knockout increased the number of cells resistant to vemurafenib, and in gray are those that decreased the frequency of either $NGFR^{HIGH}/EGFR^{HIGH}$ cells or of cells resistant to vemurafenib. As before, we organized targets into confidence tiers indicated by the number of asterisks, based on the percent of single guide RNAs against that target that showed an effect in the initial screen (see knockout color key). **b**, We performed principal component analysis of the transcriptional effects induced by the knockout of select screen targets. We used as input the gene set enrichment scores from Fig. 5a to identify primary axes that account for the greatest degree of transcriptome variability across knockout cell lines. The color indicates the effect of the knockout in the initial priming screen. The size of the dot indicates the degree of confidence we have in each particular hit based on the percent of the single guide RNAs against a target that passed a threshold of two-fold change in the initial priming screen. In black, we labeled melanoma cells where we did not knockout any targets but either enriched for $EGFR^{HIGH}$ cells, $NGFR^{HIGH}$ cells, $EGFR^{HIGH}/NGFR^{HIGH}$ cells, or for cells resistant to vemurafenib.

nature research

Corresponding author(s): Arjun Raj

Last updated by author(s): Sep 1, 2020

Reporting Summary

Nature Research wishes to improve the reproducibility of the work that we publish. This form provides structure for consistency and transparency in reporting. For further information on Nature Research policies, see Authors & Referees and the Editorial Policy Checklist.

Statistics

For all statistical analyses, confirm that the following items are present in the figure legend, table legend, main text, or Methods section.

n/a	Confirmed	
☐	☒	The exact sample size (*n*) for each experimental group/condition, given as a discrete number and unit of measurement
☐	☒	A statement on whether measurements were taken from distinct samples or whether the same sample was measured repeatedly
☐	☒	The statistical test(s) used AND whether they are one- or two-sided *Only common tests should be described solely by name; describe more complex techniques in the Methods section.*
☒	☐	A description of all covariates tested
☒	☐	A description of any assumptions or corrections, such as tests of normality and adjustment for multiple comparisons
☐	☒	A full description of the statistical parameters including central tendency (e.g. means) or other basic estimates (e.g. regression coefficient) AND variation (e.g. standard deviation) or associated estimates of uncertainty (e.g. confidence intervals)
☐	☒	For null hypothesis testing, the test statistic (e.g. *F*, *t*, *r*) with confidence intervals, effect sizes, degrees of freedom and *P* value noted *Give P values as exact values whenever suitable.*
☒	☐	For Bayesian analysis, information on the choice of priors and Markov chain Monte Carlo settings
☒	☐	For hierarchical and complex designs, identification of the appropriate level for tests and full reporting of outcomes
☐	☒	Estimates of effect sizes (e.g. Cohen's *d*, Pearson's *r*), indicating how they were calculated

Our web collection on statistics for biologists contains articles on many of the points above.

Software and code

Policy information about availability of computer code

Data collection	Microscopy data was collected using Metamorph and Elements, both commercially available. RNA-sequencing data was collected using Illumina NextSeq 500 sequencers and their accompanying software. gRNA sequencing data was collected using Illumina MiSeq instruments and their accompanying software.
Data analysis	Initial mapping of RNA sequencing data was done with open source code as described in the manuscript. All custom code used in this work can be found at https://github.com/edatorre/2020_TorreEtAl_data.git The software used for image analysis can be found at: https://github.com/arjunrajlaboratory

For manuscripts utilizing custom algorithms or software that are central to the research but not yet described in published literature, software must be made available to editors/reviewers. We strongly encourage code deposition in a community repository (e.g. GitHub). See the Nature Research guidelines for submitting code & software for further information.

Data

Policy information about availability of data

All manuscripts must include a data availability statement. This statement should provide the following information, where applicable:

- Accession codes, unique identifiers, or web links for publicly available datasets
- A list of figures that have associated raw data
- A description of any restrictions on data availability

All data used in this work can be found at: https://www.dropbox.com/sh/t08558cl4mepfm6/AABBvbtlTPSNNPoMC9NTro-9a?dl=0
RNA-sequencing data was also deposited on GEO (GSE151825, GSE149280). The gene sets used for analysis were obtained at https://www.gsea-msigdb.org/gsea/msigdb/collections.jsp#C5

Field-specific reporting

Please select the one below that is the best fit for your research. If you are not sure, read the appropriate sections before making your selection.

☒ Life sciences ☐ Behavioural & social sciences ☐ Ecological, evolutionary & environmental sciences

For a reference copy of the document with all sections, see nature.com/documents/nr-reporting-summary-flat.pdf

Life sciences study design

All studies must disclose on these points even when the disclosure is negative.

Sample size	For the primary screen, each gene was targeted with n > 6 gRNAs, which is a conservative standard in the field. Given that our targetted screen served a purpose of validation rather than discovery, and given the limitations imposed by studying rare-cell phenomena, we limited the targetted screen to n = 3 sgRNAs per target. Given that our in vivo study was a pilot study for which we did not have any prior information regarding potential effect size and variability, we did not carry out a sample size estimate. For that study, we included n = 6 mice per study group and treatment arm. We compared groups up until time points where both arms being compared had n >= 3.
Data exclusions	During our analysis, we excluded samples of poor quality or that represented a technical error. Specifically (1) throughout the analysis of NGFR-high frequency via immunofluorescence (Supplemental Figure 5) we excluded from the analysis of any sample that contained less than 500 cells given that we were calculating the frequency of an infrequent phenotype and thus a small population size would lead to misleading results. (2) During our transcriptomic analysis, we excluded from the very beginning any RNA-seq sample that was poorly represented in the data pool because low coverage of these samples could lead to apparent changes in gene expression that are rather a technical artifact due to poor sampling. (3) During our in vivo assays, we excluded two mice. One mouse (mouse_39) was excluded because it contained two tumors that merged, leading to difficulty in quantifying the trend of a single tumor. The other exclusion ("mouse_46") was done because over the course of days the tumor volume recorded decreased by >90% and then increased 10-fold, which is suggestive of a technical error in quantification rather than a biological effect.
Replication	The results of our experiments were validated in a variety of ways, always clearly indicated in the manuscript. The results from the primary screen were validated within the screen with sgRNAs targeting the same gene and outside the screen also with a secondary targeted screen. Immunofluorescence data was validated with biological triplicates using different sgRNAs (unless otherwise stated). Similarly, the transcriptomic data presented was validated with biological triplicates using different sgRNAs (unless otherwise stated). Replication efforts for each experiment are detailed throughout the manuscript.
Randomization	For the immunofluorescence experiments, all samples were randomly assigned a unique identifier that served to randomize the position of the samples throughout the workflow of staining and imaging. Similarly, to address batch effects, all transcriptomic samples were randomized across several 96-well plates. Then the sequencing libraries were built. For our in vivo experiments, we randomly assigned unique identifiers to each mice and distributed those numbers into each tumor group. For each tumor group, then we randomly assigned half of the mice to one of the treatment arms and the rest to the other treatment arm.
Blinding	In the study the investigators collecting the tumor growth data were not aware of the hypothesized drug response of each tumor group.

Reporting for specific materials, systems and methods

We require information from authors about some types of materials, experimental systems and methods used in many studies. Here, indicate whether each material, system or method listed is relevant to your study. If you are not sure if a list item applies to your research, read the appropriate section before selecting a response.

Materials & experimental systems

n/a	Involved in the study
☐	☒ Antibodies
☐	☒ Eukaryotic cell lines
☒	☐ Palaeontology
☐	☒ Animals and other organisms
☒	☐ Human research participants
☒	☐ Clinical data

Methods

n/a	Involved in the study
☒	☐ ChIP-seq
☒	☐ Flow cytometry
☒	☐ MRI-based neuroimaging

Antibodies

Antibodies used	anti-NGFR APC-labelled clone ME20.4 (Biolegend, 345107); anti-EGFR antibody clone 225 (Millipore, MABF120), donkey anti-mouse IgG-Alexa Cy3 (Jackson Laboratories, 715-545-150)
Validation	The anti-EGFR antibody clone 225 and the donkey anti-mouse IgG-Alexa Cy3 (Jackson Laboratories, 715-545-150) antibody were both validated for use in human WM989 melanoma cells by first performing the immunostains as described in the manuscript. Cells labeled as EGFR-high (based on immunofluorescence) cells were then separated from EGFR-low cells via FACS. Then, the

resulting subpopulations were fixed and RNA FISH using probes targeting EGFR transcripts was performed. Using microscopy we verified that the cells labeled as EGFR-high via immunofluorescence also contained high EGFR transcript levels. The NGFR antibody was validated for use in human WM989 cells using the same approach.

Eukaryotic cell lines

Policy information about cell lines

Cell line source(s)	We obtained patient-derived melanoma cells (WM989 and 451Lu, female and male, respectively) from the lab of Meenhard Herlyn. The HEK293T cells used for viral production were originally obtained from the lab of Junwei Shi.
Authentication	We authenticated all cell lines via Human STR profiling.
Mycoplasma contamination	All cell lines tested negative for mycoplasma.
Commonly misidentified lines (See ICLAC register)	No commonly misidentified cell lines were used in the study.

Animals and other organisms

Policy information about studies involving animals; ARRIVE guidelines recommended for reporting animal research

Laboratory animals	NOD/SCID mice (Charles River Laboratories, Wilmington, MA). Throughout the experiments, the animal facility holding rooms were maintained between 70-73F and a humidity of 30-35%. The animal holding room light schedules were on a 12 hour on and a 12 hour off schedule with lights coming on at 6:00 am and off at 6:00 pm.
Wild animals	No wild animals were used in this study.
Field-collected samples	No field-collected samples were used in this study.
Ethics oversight	All animal experiments were approved by Wistar's Institutional Animal Care and Use Committee (IACUC) (IACUC #112503X_0) and were performed in an Association for the Assessment and Accreditation of Laboratory Animal Care (AAALAC) accredited facility.

Note that full information on the approval of the study protocol must also be provided in the manuscript.